



Stabilization and evolution of the Brazilian subcontinental lithospheric mantle: Insights from garnet xenocrysts and peridotite xenoliths of Três Ranchos kimberlite (APIP, Brazil)

Vincenza Guarino^{a,*}, Mattia Bonazzi^b, Paolo Nimis^c, Rogério Guitarrari Azzone^d, Bruna Cariddi^{a,e}, Alberto Zanetti^b

^a Dipartimento di Scienze della Terra, dell'Ambiente e delle Risorse, Università di Napoli Federico II, Complesso Universitario Monte Sant'Angelo, Via Cintia 21, 80126 Naples, Italy

^b Istituto di Geoscienze e Georisorse, CNR, Pavia, Via Ferrata, 1, 27100 Pavia, Italy

^c Dipartimento di Geoscienze, Università di Padova, via G. Gradenigo 6, 35131 Padova, Italy

^d Instituto de Geociências, Universidade de São Paulo, Rua do Lago 562, Cidade Universitária, 05508-900 São Paulo, Brazil

^e Istituto Nazionale di Geofisica e Vulcanologia, sezione di Napoli Osservatorio Vesuviano, Via Diocleziano 328, 80124 Napoli, Italy

ARTICLE INFO

Article history:

Received 14 March 2023

Revised 17 October 2023

Accepted 14 January 2024

Available online 19 January 2024

Handling Editor: S. Tappe

Keywords:

Thermal structure

Chemical zoning

Subcontinental lithospheric mantle

Garnets

Laser analyses

Peridotite

Kimberlite

Brazil

ABSTRACT

The thermal structure and chemical composition of the subcontinental lithospheric mantle beneath the Alto Paranaíba Igneous Province defined by the major and trace element compositions of garnet and clinopyroxene xenocrysts and mantle peridotite xenoliths entrained in the Cretaceous Três Ranchos kimberlite. Estimated temperatures and pressures indicate a typical cratonic geotherm, with a surface heat flow of $\sim 40 \text{ mW/m}^2$ slightly hotter than that at the São Francisco Craton margin ($35\text{--}36 \text{ mW/m}^2$), suggesting lateral heterogeneities in the geothermal gradients. A deep mantle portion (160 km) is recorded by a lherzolite xenolith (5 GPa and 1200 °C). This portion has undergone pervasive interstitial melt percolation of an ultra-alkaline silicate melt and late injection of small silicate melt fractions such as the host carbonated kimberlite. This pervasive migration extended into shallower SCLM sectors at 124–100 km (3.9–3.1 GPa and $\sim 940\text{--}810 \text{ °C}$) as evidenced by metasomatized (\pm phlogopite) peridotite identified by sinusoidal REE garnet compositions. This portion is apparently intercalated at 120–110 km depth (3.7–3.3 GPa and $\sim 850 \text{ °C}$) with strongly depleted peridotites showing garnet and clinopyroxene compositions extremely impoverished in moderately incompatible elements, as a result of extreme ancient, melt extraction. Atop the metasomatized and depleted peridotites, at 100 km depth, a layer of fertile lherzolite is identified by garnet xenocrysts, with 'normal', HREE-enriched, steadily fractionated LREE-depleted patterns. Combining our data with those of the Osvaldo França SCLM points to the occurrence of a deeper sector ($>100 \text{ km}$ depth beneath Três Ranchos) originally formed by extremely depleted peridotites, successively metasomatized by ultra-alkaline melts; and a shallower sector of the São Francisco craton composed of fertile lherzolites unrelated to ultra-alkaline magmatism. Similar fertile lherzolites are found in the uppermost sectors of the Siberian and Kaapval SCLM, suggesting that they may be a ubiquitous, primary feature, possibly related to the stabilization of the Archean cratons.

© 2024 The Author(s). Published by Elsevier B.V. on behalf of International Association for Gondwana Research. This is an open access article under the CC BY license (<http://creativecommons.org/licenses/by/4.0/>).

1. Introduction

Kimberlites are rare rocks that occur exclusively in cratonic and pericratonic areas. Kimberlitic melts, during rapid magma ascent from the base of the subcontinental lithosphere (150–200 km depth; Mitchell, 1986; Nowell et al., 2004; Sparks et al., 2006), carry up a large cargo of mantle debris (as xenoliths and xeno-

crysts, including diamonds), as well as crustal xenoliths. They experienced a variety of open system processes, including assimilation of phenocrysts and groundmass crystallized from different kimberlite magmas and from the mantle they crossed, and mixing of volatile components (mostly F, H₂O, and CO₂). Kimberlites may also experience contamination by crustal material, as well as textural variations associated with mantle material entrapment, reworking processes, and weathering. They are often affected by deuteric alteration due to the very large amount of contained volatiles. Thus, the kimberlites are typically hybrid in nature, making it

* Corresponding author.

E-mail address: vincenza.guarino@unina.it (V. Guarino).

difficult to infer the composition of the primitive magmas and melt components (Patterson et al., 2009). Typical mantle debris identified in the kimberlites are peridotite xenoliths and xenocrysts derived from their fragmentation. In particular, the high resistance of garnet xenocrysts to magmatic resorption and weathering favors its preservation in kimberlites. Moreover, the major and minor element composition of garnets is indicative of pressure and temperature conditions and type of disrupted peridotite (Iherzolite, harzburgite, wehrlite, etc.), while the trace element concentration and fractionation can provide valuable constraints on evolution processes of lower lithosphere (partial melting, metasomatism, re-fertilization, exsolution). Therefore, mantle garnets are a very important source of information on the nature, thermal state, and chemical evolution processes of the Subcontinental Lithospheric Mantle (SCLM; Nowicki et al., 2007).

The Late Cretaceous Alto Paranaíba Igneous Province (APIP; ~91–78 Ma; Guarino et al., 2013; Takenaka et al., 2023) is NW–SE trending and is located between the NE margin of the Paraná Basin and the SW margin of the São Francisco Craton, crossing SE Minas Gerais and SW Goiás on the Brasília Belt, a Late Precambrian mobile belt (Almeida et al., 2000; D'Agrella-Filho et al., 2011; Peucat et al., 2011, and references therein; Fig. 1). This province covers an area of ~20,000 km² and is characterized by the emplacement of kimberlites, together with abundant lava flows, plugs, intrusions and pyroclastic rocks of kamafugitic, lamprophyric and carbonatitic compositions (Gibson et al., 1995; Brod

et al., 2000; Araújo et al., 2001; Read et al., 2004; Gomes and Comin-Chiaromonti, 2005; Melluso et al., 2008; Guarino et al., 2013, 2017, 2021; Coldebella et al., 2020; Lima et al., 2020; Carvalho et al., 2022a,b; Azzone et al., 2022). Kimberlite intrusions were also identified in the southernmost part of Brazil (Lages, Santa Catarina State; Barabino et al., 2007). In the APIP, Cabral Neto et al. (2017) identified the Coromandel-Três Ranchos field, which covers an area of approximately 11,600 km². This area contains more than five hundred intrusions of kimberlitic affinity, emplaced as diatremes, pipes and dikes, with surface areas ranging from less than 1 ha to 360 ha. The Três Ranchos kimberlite samples discussed in this manuscript are fragments coming from the same kimberlite intrusion (sample TR 14) that was first studied by Melluso et al. (2008) and Guarino et al. (2013). It has an emplacement age of 87 ± 3 Ma (U–Pb perovskite age; Guarino et al., 2013).

We report new major and trace element analyses of garnet and clinopyroxene xenocrysts, and of all minerals identified in the peridotite xenoliths (dunite, harzburgite, Iherzolite a garnet-phlogopite-spinel xenoliths) entrained in the Três Ranchos kimberlite. We also report new mineral analyses in the kimberlite matrix. These data will be used to constrain the chemical features, evolution stages, and thermal structure of the Brazilian SCLM beneath the APIP during Mesozoic–Cenozoic break-up of western Gondwana. By analyzing the thermal and chemical zoning of the lithospheric column beneath the APIP (considering the Três Ranchos, Osvaldo França 1, and Canastra 8 kimberlites) and the State of

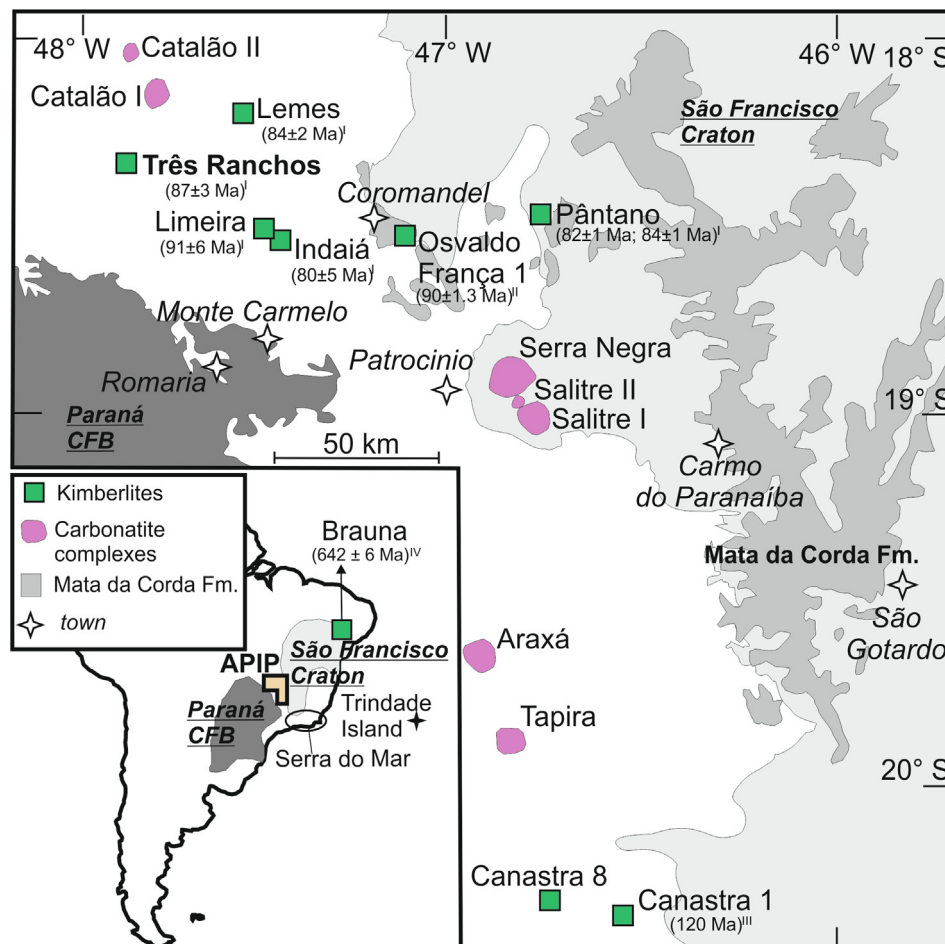


Fig. 1. Localization of major kimberlite intrusions in the Late Cretaceous Alto Paranaíba Alkaline Province, southern Brazil (modified after Guarino et al., 2013). Ages are from Guarino et al., 2013 (^I); Carvalho et al., 2022a (^{II}); Pereira, 2007 and references therein (^{III}); Donatti-Filho et al., 2013 (^{IV}). Inset: Location of the Brauna kimberlite intrusion in the northeastern part of the São Francisco Craton, Paraná CFB (Continental Flood Basalts), Trindade Island, Serra do Mar province and APIP (Alto Paranaíba Alkaline Province).

Bahia (Brauna kimberlite) in the northeastern sector of the São Francisco Craton, we will provide an insight into the stabilization processes and evolution of the Brazilian SCLM.

2. The Três Ranchos kimberlite

The Três Ranchos kimberlite (also known as Fazenda Alagoinha and Três Ranchos-IV; Table 1) is a well-known APIP occurrence. It outcrops as disrupted blocks in an area of about 0.5 ha consisting of dark to gray/green fresh homogeneous rocks with inequigranular textures characterized by hypabyssal facies features. The rocks have been classified as Group-I coherent macrocrystic kimberlite (Guarino et al., 2013), and exhibit a porphyritic to seriate texture, with abundant megacrysts and macrocrysts of olivine, phlogopite, chromite, and garnet, set in a fine-grained matrix formed by microcrysts of serpentine, carbonates, perovskite, phlogopite, Cr-spinel, magnetite, potassic richterite, apatite, and barite (Melluso et al., 2008; Guarino et al., 2013). It is considered one of the 'archetypal' kimberlites from the APIP (Azzone et al., 2022). The Três Ranchos kimberlite intrudes granitic rocks of the Monte Carmelo complex (Neoproterozoic), and quartzites, schists, and amphibolites of the Araxá Group (Neoproterozoic), which also occur as xenoliths in the kimberlite (Costa et al., 1996; Cabral Neto et al., 2017). Micro-diamonds were reported in this intrusion by Gonzaga et al. (1994). Centimeter-sized xenoliths of dunites, harzburgites and lherzolites, mostly serpentinized and/or carbonatized, have been also reported.

3. Materials and methods

In this study, we have analyzed 10 garnet and 1 clinopyroxene xenocrysts and individual minerals (olivine, orthopyroxene, clinopyroxene, garnet, spinel and phlogopite) in 1 dunite, 2 harzburgites, 1 lherzolite and 1 garnet-phlogopite-spinel xenoliths from several Três Ranchos kimberlite samples (TR8, TR11, TR9, TR4, TR10, TR2a, TR2b, TR2c; Suppl. Fig. 1). Additional mineral phases (olivine, phlogopite, perovskite, amphibole, oxides, carbonates, and apatite) were analyzed in the kimberlite samples TR8 and TR10, greatly expanding the data set available in the literature (Melluso et al., 2008; Guarino et al., 2013). Samples TR8, TR11, TR9, TR4, TR10, TR2a, TR2b, and TR2c analyzed in this manuscript, as well as samples TR14 and TR16 analyzed in Melluso et al. (2008)

and Guarino et al. (2013), are all from the same Três Ranchos kimberlite (sample TR14; Melluso et al., 2008; Suppl. Table 1).

Mineral chemical compositions were determined on polished and carbon-coated thin sections at the Dipartimento di Scienze della Terra, dell'Ambiente e delle Risorse (DiSTAR), University of Naples Federico II (Italy), using a JEOL JSM-5310 microscope and an Oxford Instruments Microanalysis Unit, equipped with an INCA X-act detector. The operating conditions were 15 kV primary beam voltage, 50–100 μ A filament current, spot size of 5–10 μ m, 20 mm working distance and 50 s net acquisition real time. An INCA X-stream pulse processor with INCA Energy software was used for the measurements. Energy uses the XPP matrix correction scheme, developed by Pouchou and Pichoir (1988) and the Pulse Pile up correction. Quant optimization is performed using cobalt (FWHM - full width at half maximum peak height - of the strobed zero = 60–65 eV). The following standards from the Smithsonian Institute were used for calibration: diopside (Ca K α), San Carlos olivine (Mg K α), anorthoclase (Al K α , Si K α), albite (Na K α), rutile (Ti K α), fayalite (Fe K α), Cr₂O₃ (Cr K α , chromite), rhodonite (Mn K α), orthoclase (K K α), apatite (P K α), fluorite (F K α), barite (Ba L α), celestine (Sr L α), zircon (Zr L α , Hf L α), synthetic Smithsonian orthophosphates (REE L α , Y L α), pure vanadium, niobium, and tantalum (V L α , Nb L α , Ta L α), pyrite (S K α), sphalerite (S K α , Zn K α), galena (Pb K α), chalcopyrite (Cu K α), and sodium chloride (Cl K α). The mineral standards used are reported in Guarino et al. (2021) and Melluso et al. (2022). Additional kelyphitic coronas around garnet xenocrysts in the Três Ranchos kimberlite were analyzed at the University of São Paulo (Brazil). Electron microprobe (EMP) analyses were performed by wavelength-dispersive X-ray spectroscopy (WDS) using a Jeol JXA-8600 at the GeoAnalítica Core Facility of the Instituto de Geociências. The electron microprobe is equipped with five wavelength-dispersive spectrometers with the following pairs of analytical crystals **TAP/STE**, **TAP/PET**, **LIF/PET**, **PET/LIF** and **LIF/PET**, respectively (crystals in bold were used in the routines of this study). Operating conditions were 15 kV accelerating potential, 20 μ A probe current, and about 1–5 μ m beam diameter. Peak count times ranged from 10 s for most major elements to 20 s for minor and trace elements. Similar standards, most from the Smithsonian Institute, were used for calibration.

Trace element concentrations were determined in xenocrysts, phenocrysts, and mantle xenoliths (Suppl. Tables 2 to 5) by in-situ LA-ICP-QQQ-MS analysis at the Istituto di Geoscienze e Georisorse (IGG), Consiglio Nazionale delle Ricerche (CNR) of Pavia (Italy). The instrumentation consists of a Triple Quadrupole ICP-MS

Table 1
Previous works on the Três Ranchos kimberlite, one of APIP's best known occurrences.

	Reference	Classification / Nomenclature	Facies/Body	Observations
Três Ranchos	Gonzaga & Tompkins (1991)	Kimberlite		diamondiferous kimberlite
	Danni et al. (1991)	Kimberlite	pipe	not consistent with evolution of typical kimberlites (kamafugitic affinity); Fazenda Alagoinha intrusion
	Gibson et al. (1995b)	Kimberlite	pipe	breccia structure; fragments of carbonated granite
	Carlson et al. (1996)	Kimberlite	hypabyssal	
	Costa et al. (1997)	Kimberlite	hypabyssal	dike associated
	Melluso et al. (2008)	Kimberlite	hypabyssal	
	Guarino et al. (2013)	Kimberlite	hypabyssal	
	Felgate (2014)	Kimberlite	hypabyssal	
	Lim et al. (2018)	Kimberlite	pipe-filing coherent	phlogopite carbonate-serpentine kimberlite
	Coldebella et al. (2020)	Kimberlite	hypabyssal	
	Azzone et al. (2022)	Kimberlite	hypabyssal	APIP "archetypal"-type

Table 2

P–T estimates for the studied xenoliths and xenocrysts.

Sample	Type	Minimum P (GPa)	P (GPa)	T (°C)	Depth
TR LH1	Lherzolite xenolith		5.1 ^[1]	1197 ^[1]	162
TR2a HZ2	Harzburgite xenolith		3.9 ^[2]	926 ^[2]	124
TR8 grt1	Grt xenocryst	3.6 ^[3]	3.8 ^[4]	938 ^[5]	120
TR11 grt	Grt xenocryst		3.7 ^[3]	911 ^[5]	117
TR2c grt2 xen	Grt–Phl–Spl xenolith		3.4 ^[3]	903 ^[5]	108
	Grt xenocryst				
TR8 grt2	Grt xenocryst	2.6 ^[3]	3.4 ^[4]	856 ^[5]	108
TR2a cpx xen	Cpx xenocryst		3.3 ^[1]	854 ^[1]	105
TR8 grt3	Grt xenocryst	3.2 ^[3]	3.2 ^[4]	819 ^[5]	101
TR10 grt1	Grt xenocryst	2.1 ^[3]	3.3 ^[4]	832 ^[5]	105
TR10 grt2	Grt xenocryst	2.1 ^[3]	3.2 ^[4]	813 ^[5]	101
TR9 grt	Grt xenocryst	3.2 ^[3]	3.1 ^[4]	811 ^[5]	98
TR4 grt	Grt xenocryst	2.1 ^[3]	3.2 ^[4]	826 ^[5]	101
TR2b grt	Grt xenocryst	2.2 ^[3]	3.3 ^[4]	837 ^[5]	105
TR2c grt1	Grt xenocryst	2.2 ^[3]	3.3 ^[4]	834 ^[5]	105

^[1] P–T: combination of the enstatite-in-clinopyroxene thermometer and Cr-in-clinopyroxene barometer of Nimis and Taylor (2000).^[2] P–T: combination of the Ni-in-garnet thermometer (see above) and the Nickel and Green (1985) orthopyroxene-garnet barometer.^[3] P: Cr-in-garnet barometer of Grütter et al. (2006).^[4] P: projecting the garnet temperatures onto the geotherm (Ryan et al., 1996).^[5] T: Ni-in-garnet thermometer [average Ryan et al. (1996) and Canil (1999)].

Agilent Series 8900 coupled with Q-switched Nd:YAG laser source, model Brilliant (Quintel, France), whose fundamental emission (1064 nm) is converted to 266 nm by two harmonic generators. The laser was operated at 10 Hz, ≤ 3.5 mW power, 50 μ m spot diameter at the target surface. Helium was used as the carrier gas, which was mixed with Ar downstream of the ablation cell in an almost 1:1 ratio. Data reduction was performed using the 'Glitter' software package (Van Achterbergh et al., 2001), with the synthetic glass NIST SRM 610 (Pearce et al., 1997) as the external standard (Suppl. Table 6). The internal standards used were ²⁹Si for olivine, orthopyroxene and phlogopite, and ⁴⁴Ca for clinopyroxene and garnet. The same integration intervals and spot sizes were used for both standards and unknowns. Precision and accuracy were evaluated by repeated analysis of the USGS BCR-2 g reference sample (Suppl. Table 6), which was better than ± 10 % at the ppm concentration level.

3.1. Thermobarometry

Pressure (P) and temperature (T) estimates for the Três Ranchos xenoliths and xenocrysts were obtained by using combinations of different thermobarometers. Since only part of the original mineral assemblages was preserved, it was impossible to use the same thermobarometric combination for all the samples. Therefore, to ensure consistency among the different P–T estimates, thermobarometric methods that were shown to be mutually consistent were generally preferred. This excluded, for instance, the various versions of the orthopyroxene-garnet Fe–Mg-exchange thermometer. In particular, the version proposed by Harley (1984) for this thermometer is known to overestimate at low T and underestimate at high T (Nimis and Grütter, 2010). The version proposed by Nimis and Grütter (2010) is known to produce excessive scatter (Nimis et al., 2020). We also found that the more recent version of Sudholz et al. (2022), which relies on an unusual thermometric expression, may also produce excessive scatter when applied to natural samples.

Temperatures for most of the studied samples were obtained by using the Ni-in-garnet thermometer (Ryan et al., 1996; Canil, 1999; Sudholz et al., 2021). Although the consistency between the different versions of this thermometer and other well-tested thermometers for peridotites is still not satisfactory (cf. Fig. 7 in Sudholz et al., 2021), this thermometer has the advantage of being independent on P. Therefore, uncertainties in P estimates do not propagate

any additional errors on the thermometric estimates. Moreover, garnets are present in most of the studied xenoliths and xenocrysts, thus ensuring consistency among T estimates over most of our dataset. In this paper, we will follow the suggestion of Czás et al. (2020) and Nimis et al. (2020) that averaging $T_{\text{Ryan et al. (1996)}}$ and $T_{\text{Canil (1999)}}$ produces T estimates that are more consistent with those obtained for clinopyroxenes.

For the garnet xenocrysts and the garnet-phlogopite-spinel xenolith TR2c, P estimates were obtained by using the Cr-in-garnet barometer of Grütter et al. (2006). This barometer underestimates P for garnets that are not in equilibrium with spinel. When the presence of spinel in the original mineral assemblage is unknown, as it is the case for all the garnet xenocrysts, this method produces minimum P estimates. If the local geotherm is known and the garnets are assumed to have last equilibrated along this geotherm, their true equilibrium P can then be retrieved by projecting the garnet temperatures onto the geotherm (Ryan et al., 1996). For comparative purposes, a similar procedure was applied also on published garnet xenocryst data from other areas of the APIP (Carvalho et al., 2022a).

As for harzburgite TR2a HZ2, lherzolite TR LH1 and clinopyroxene xenocryst TR2a, both P and T could be directly estimated, without requiring projection on a geotherm. P–T estimates for harzburgite TR2a HZ2 were obtained by using a combination of the Ni-in-garnet thermometer (see above) and the Nickel and Green (1985) orthopyroxene-garnet barometer. Since the molar content of Na in the orthopyroxene did not exceed the sum of Cr and Ti, no correction for the expression of the activity of the Mg-Tschermak component was necessary (cf. Carswell, 1991). P–T estimates for clinopyroxene in lherzolite TR LH1 and clinopyroxene xenocryst TR2a were obtained by using a combination of the enstatite-in-clinopyroxene thermometer and Cr-in-clinopyroxene barometer of Nimis and Taylor (2000). To ensure better consistency between the clinopyroxene and orthopyroxene-garnet barometers, the Cr-in-clinopyroxene barometer was corrected as suggested by Nimis et al. (2020). The clinopyroxene compositions were checked for analytical quality, equilibrium with garnet and orthopyroxene, and predicted P estimate quality as recommended by Ziberna et al. (2016). This screening excluded the interstitial clinopyroxene in harzburgite TR4 HZ1 from the calculations. Clinopyroxene rims in sample TR LH1 were found to be very poor in Cr₂O₃, (ca. 0.2 wt%), clearly indicating disequilibrium with garnet. Therefore, only core analyses were considered.

Typical uncertainties on P and T estimates, considering propagation of both calibration and analytical errors, are of ca. 0.4 GPa and 50 °C (Ryan et al., 1996; Nimis and Grütter, 2010).

4. Results

4.1. Petrographic, geochemical, and mineralogical features of Três Ranchos kimberlite and its xenoliths

4.1.1. Três Ranchos kimberlite

The Três Ranchos kimberlite rock is ultrabasic, ultramafic, and potassic with high concentrations of Rare Earth Elements ($\Sigma\text{REE} = 1400$ ppm), very high La_N/Yb_N (225; subscript N indicates normalization to the chondrite composition) and other trace elements (e.g., Cr, Ni, Nb, Zr, Sr, and Ba; see Suppl. Table 1; Melluso et al., 2008; Guarino et al., 2013). This sample is uncontaminated, with a Contamination Index $[\text{C.I.} = (\text{SiO}_2 + \text{Al}_2\text{O}_3 + \text{Na}_2\text{O}) / (\text{MgO} + 2^*\text{K}_2\text{O})] = 1.1$ (Clement, 1982; Nowicki et al., 2008). The samples studied contain large olivine xenocrysts with high forsterite content [Fo_{93-91} , where $\text{Fo} = 100 \times \text{Mg}/(\text{Mg} + \text{Fe})$ in atoms] plus phenocryst assemblages made up of olivine (Fo_{88-89} ; Suppl. Table 7) and very Cr-rich spinel [$\text{Cr}\# = 100 \times \text{Cr}/(\text{Cr} + \text{Al}) = 76-82$] set in a microcrystalline groundmass made up of olivine, serpentine, tetraferriphlogopite [$\text{Mg}\# = 100 \times \text{Mg}/(\text{Mg} + \text{Fe}) = 84-94$ with Fe^{3+} in the tetrahedral site (0.06–0.35 apfu) and BaO up to 10.2 wt%], perovskite with loparite component [$(\text{Ce}, \text{Na}, \text{Ca})_2(\text{Ti}, \text{Nb})_2\text{O}_6 = 7-23$ mol%], magnesio-chromite to chromite ($\text{Cr}\# = 73-95$; $\text{Mg}\# = 35-56$), magnesian Cr-magnetite ($\text{MgO} = 4.8-7.7$ wt%; $\text{Cr}_2\text{O}_3 = 0.3-1.9$ wt%), potassic richterite ($\text{Mg}\# = 94$), apatite, calcite, and strontianite (Suppl. Tables 4 and 7).

4.1.2. Peridotite xenoliths and clinopyroxene xenocryst

Dunite, harzburgite, and lherzolite xenoliths, together with a garnet-phlogopite-spinel xenolith and a clinopyroxene xenocryst, were identified in the studied thin sections of several Três Ranchos kimberlite fragments.

The dunite xenolith TR9 DN (Suppl. Fig. 1c) is characterized by rounded olivine grains, larger than 1 cm, undeformed and with a coherent extinction. It is unzoned and forsteritic (Fo_{92} ; Suppl. Table 2).

The harzburgite xenolith TR4 HZ1 (Fig. 2a) has a porphyroclastic texture consisting of coarse-grained olivine and orthopyroxene. The rounded olivines have a variable extinction from kink-bands to wavy. They are unzoned and forsteritic (Fo_{91-93} ; Suppl. Table 2). The rounded orthopyroxenes are slightly deformed and have wavy extinction. They have high $\text{Mg}\#$ (92–93) and low concentrations of Al ($\text{Al}_2\text{O}_3 = 0.2-0.4$ wt%) and Cr ($\text{Cr}_2\text{O}_3 = 0-0.3$ wt%) (Suppl. Table 3). Newly formed clinopyroxene ($\text{Mg}\# = 87$) was identified in the interstitial position (Suppl. Table 3; Fig. 2a).

A strongly altered clinopyroxene xenocryst (TR2a cpx xen; Fig. 2b) has high $\text{Mg}\#$ (93–94) and enriched in Cr_2O_3 (1.4–1.5 wt%).

The harzburgite xenolith TR2a HZ2 (Fig. 2c,d) is characterized by undeformed olivines with coherent extinction and no kink-bands. These olivines have a high forsterite content (Fo_{92-93} ; Suppl. Table 2). Orthopyroxene ($\text{Mg}\# = 92-94$) is undeformed, with the presence of minor exsolutions (Suppl. Table 3). Garnets ($\text{Mg}\# = 79-80$), identified in the interstitial position, are characterized by low CaO (4.6–4.9 wt%) and Cr_2O_3 (1.4–1.9 wt%) concentrations (Suppl. Table 5; Fig. 2c,d).

The lherzolite xenolith TR LH1 (Fig. 3a-d) is characterized by a porphyroclastic texture consisting of coarse-grained olivine, orthopyroxene, and clinopyroxene. The olivines are rounded, showing wavy extinction on crossed nicols, while kink-bands are not observed. The coarse pyroxenes (about 25 % by volume) also display a wavy extinction. Clino- and ortho-pyroxenes also occur

as anhedral interstitial crystals or, subordinately, as rounded grains partially replacing olivine. The presence of exsolution lamellae is limited and the orthopyroxene/clinopyroxene ratio is close to 1. The coarse olivine and pyroxenes are variably replaced along the grain boundaries and interstices by a very fine-grained mineral assemblage (mostly tens of microns in size) consisting of newly formed olivine, clinopyroxene, phlogopite, perovskite, rutile surrounded by ilmenite, and altered apatite (Fig. 3b-d; Suppl. Table 8). There is no clear petrographic evidence of percolation of the host kimberlite into the xenolith, suggesting that also the second melt injection took place prior to entrainment of the xenoliths in the ascending melt.

Trails and clouds of micron-scale inclusions, apparently related to late rock-melt interaction, are present in the coarse olivines and pyroxenes, and are particularly abundant in the clinopyroxenes, which sometimes appear completely cloudy. The large olivines are unzoned and forsteritic (Fo_{91-92} ; Fig. 3a-d; Suppl. Table 2), while clinopyroxene (diopside) and orthopyroxene (enstatite) have slight compositional differences between core and rim. Clinopyroxene cores are characterized by slightly higher $\text{Mg}\#$ (91–93) than the rims ($\text{Mg}\# = 90-92$). The Al and Cr concentrations are variable, but they do not vary systematically from the core to the rim ($\text{Al}_2\text{O}_3 = 0.2-2.3$ wt% and $\text{Cr}_2\text{O}_3 = 1.2-1.8$ wt%; Suppl. Table 3). Similarly, the orthopyroxene cores have a higher $\text{Mg}\#$ (93) than the rims ($\text{Mg}\# = 92$; Suppl. Table 3). The Al and Cr concentrations do not vary systematically, but the maximum values are higher in the rim ($\text{Al}_2\text{O}_3 < 1.05$ wt% and $\text{Cr}_2\text{O}_3 < 0.32$ wt%) than in the core ($\text{Al}_2\text{O}_3 < 0.64$ wt% and $\text{Cr}_2\text{O}_3 < 0.13$ wt%). Interstitial fine-grained clinopyroxene (diopside) is a relatively Fe-rich and Al-Cr-poor diopside ($\text{Mg}\# = 89$; $\text{Al}_2\text{O}_3 < 0.2$ wt%; Cr_2O_3 below the detection limit of the electron microprobe). Mica is tetraferriphlogopite ($\text{Mg}\# = 91-93$) with significant Fe^{3+} in the tetrahedral site (0.11–0.14 apfu). Perovskite ($\text{CaTiO}_3 = 85-93$ mol%) is characterized by variable amounts of REE and Nb ($\Sigma\text{REE}_2\text{O}_3 = 1.3-5.8$ wt%; $\text{Nb}_2\text{O}_5 = 1.4-2.1$ wt%; Suppl. Table 8), indicating a significant amount of loparite ($\text{CeNaTi}_2\text{O}_6 = 2-9$ mol%) and lueshite ($\text{NaNbO}_3 = 1.4-2.4$ mol%) components.

4.1.3. A garnet-phlogopite-spinel xenolith

The TR2c xenolith consists of pyropic garnet largely overgrown by phlogopite with minor chromite ($\text{Cr}_2\text{O}_3 = 43.0-45.2$ wt%; Fig. 3e, f; Suppl. Table 4). The phlogopites ($\text{Mg}\# = 86-89$) are characterized by high Cr concentration ($\text{Cr}_2\text{O}_3 = 1.2-2.6$ wt%), whereas the garnets ($\text{Mg}\# = 81-82$) have limited variation in CaO (6.5–6.7 wt%) and Cr_2O_3 (7.2–8.0 wt%) concentrations.

4.1.4. Garnet xenocrysts

The garnet xenocrysts are variable in size and shape, ranging from rounded to anhedral and fractured, with distinct dark kelyphitic corona, which is absent only around the TR8 grt2 xenocryst (Figs. 4 and 5). The TR9 garnet contains minute Cr-bearing phlogopites ($\text{Cr}_2\text{O}_3 = 1.3-1.7$ wt%; Fig. 4e). The few analyses obtained on the kelyphitic coronas indicate the presence of phlogopite, but with low K_2O concentrations (5.4–9.8 wt%) and rich in F (0.5–1.3 wt%; Suppl. Table 9). The analyzed garnet xenocrysts have markedly variable concentrations of Cr_2O_3 (1.9–10.9 wt%) and CaO (4.5–9.1 wt%) with $\text{Mg}\#$ values of 77–81 (Suppl. Table 5). All garnet xenocrysts are unzoned.

The $\text{Mg}/(\text{Mg} + \text{Fe})$ and $\text{Ca}/(\text{Ca} + \text{Mg})$ values indicate that all the studied garnets are of mantle origin (Fig. 6a; Suppl. Table 5). In the CaO vs. Cr_2O_3 plot (Grütter et al., 2004), these garnets, like other Três Ranchos garnet xenocrysts (Coldebella et al., 2020) fall in the lherzolitic field, indicating that their protoliths were saturated in or close to saturation with clinopyroxene (Fig. 6b). Only one wehrlitic garnet (TR11 grt) was identified in this study (Fig. 6b). According to this classification, literature garnet xenocrysts from

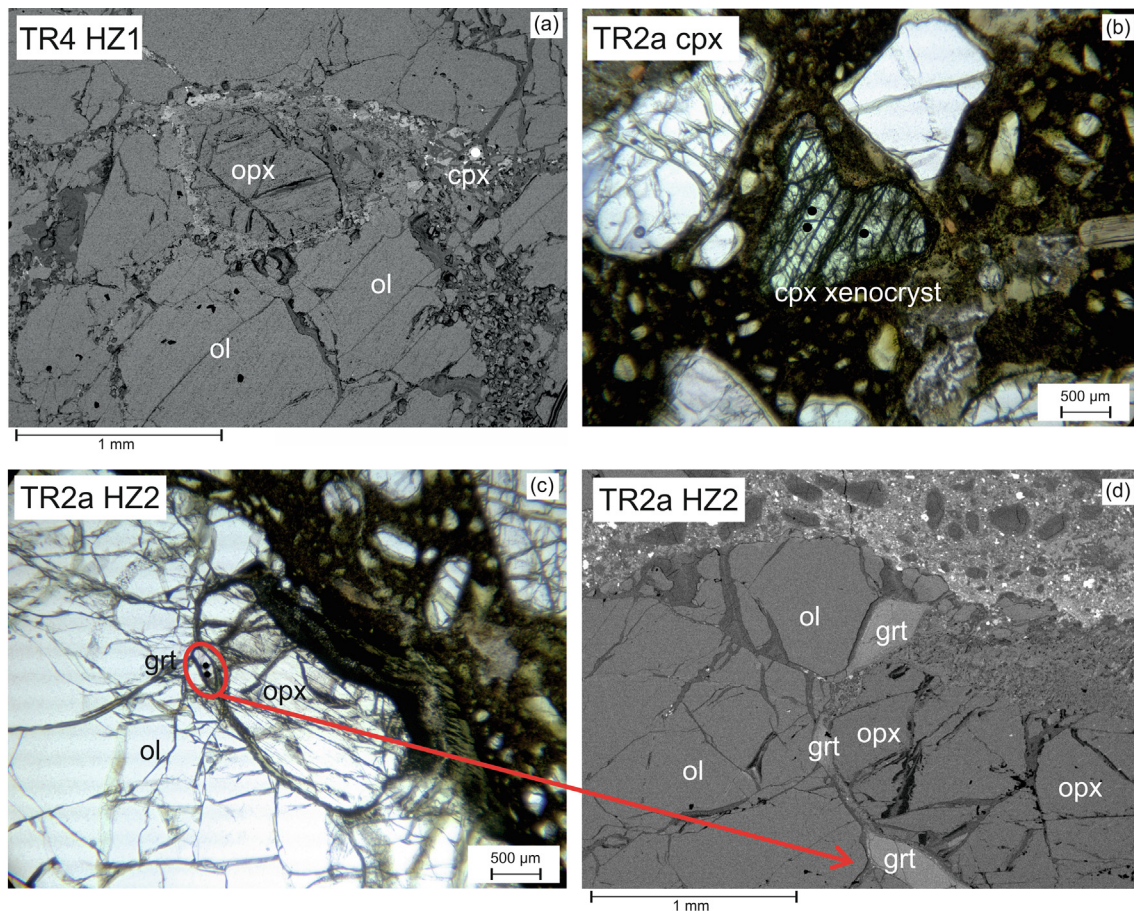


Fig. 2. Back-scattered electron images and thin section photomicrographs illustrating the main petrographic features of the harzburgite TR4 HZ1 (a), clinopyroxene xenocryst TR2a (b) and harzburgite TR2a HZ2 (c–d). Abbreviations used: cpx, clinopyroxene; grt, garnet; ol, olivine; opx, orthopyroxene (Warr, 2021).

the Brauna kimberlite field are mainly *lherzolitic* and *pyroxenitic*, those from the Canastra 8 kimberlite are *harzburgitic* and *lherzolitic*, and those from the Osvaldo França 1 kimberlite are mainly *lherzolitic* (Donatti-Filho et al., 2013; Hill et al., 2015; Carvalho et al., 2022a; Fig. 6b).

4.2. Trace element concentrations in mineral phases

4.2.1. LA-ICP-MS analyses in the clinopyroxene xenocryst, peridotite xenoliths and phlogopites in the host kimberlite

The TR2a clinopyroxene xenocryst in the REE and multi-element normalized patterns is less enriched in all incompatible elements and has $V_N/Sc_N > 1$ (Fig. 7).

The REE and multi-element normalized patterns (Suppl. Fig. 2a, b) of the TR LH1 olivines have low abundances in all incompatible elements, with slight enrichments from core to rim, and $V_N/Sc_N < 1$. The REE and multi-element normalized patterns (Suppl. Fig. 2c,d) of the cloudy TR LH1 orthopyroxenes have relative enrichments in highly incompatible elements, such as LREE, while Y and HREE are very low or below the detection limits (Yb and Lu). The V_N/Sc_N ratio is > 1 .

The TR LH1 clinopyroxenes have strongly fractionated LREE-enriched normalized patterns (with $La_N/Yb_N \sim 50\text{--}698$; Fig. 7), the clinopyroxene rims are on average more REE-enriched than those in the MARID (Mica-Amphibole-Rutile-Ilmenite-Diopside) and PIC (Phlogopite-Ilmenite-Clinopyroxene) clinopyroxene fields (Fig. 7; Fitzpayne et al., 2018), although the overall shapes are similar to those in MARID. The multi-element patterns have similar

fractionation and variation of an order of magnitude variation in the La–V interval (Fig. 7). The V_N/Sc_N ratio is > 1 . The variation of Cs, Rb, Ba, Th, U, Nb, and Ta is significantly greater, with the higher concentrations far exceeding those found in both MARID and PIC clinopyroxenes (Fig. 7). Zirconium and Hf define a trough similar to the MARID clinopyroxenes. However, the magnitude of the trough is smaller for Ti.

Phlogopites from the host kimberlite have very low REE contents (Suppl. Fig. 2e) and the typical enrichments in Cs, Rb, Ba, Th, U, Nb, Ta, and Ti in the multi-element normalized patterns (Suppl. Fig. 2f). The V_N/Sc_N ratio is > 1 .

4.2.2. LA-ICP-MS analyses of garnets and phlogopites in garnet-phlogopite-spinel xenolith

The analyzed garnets in the garnet-phlogopite-spinel (grt-phl-sp) xenolith TR2c (Fig. 3e,f) are characterized by a very unusual, extremely depleted REE pattern, which are only in the Y (having Y geochemical behavior in between that of Ho and Er) to Lu region above the detection limits (Fig. 8a,b). The same is observed in their multi-element patterns (Fig. 8d,e). The phlogopites in this xenolith have the least enriched REE and multi-element normalized patterns, and V_N/Sc_N is > 1 (Suppl. Fig. 2e).

4.2.3. LA-ICP-MS analyses of garnet xenocrysts

The garnet xenocrysts exhibit LREE-depleted ($La_N/Yb_N \leq 0.39$) normalized patterns with variable concentration and fractionation (e.g., Y ranges from 0.6 to 30.7 ppm; Fig. 8). The TR10 grt1, TR10 grt2, TR4 grt, TR2b grt, and TR2c grt1 have a 'normal', HREE-enriched, steadily fractionated REE pattern, characterized by high

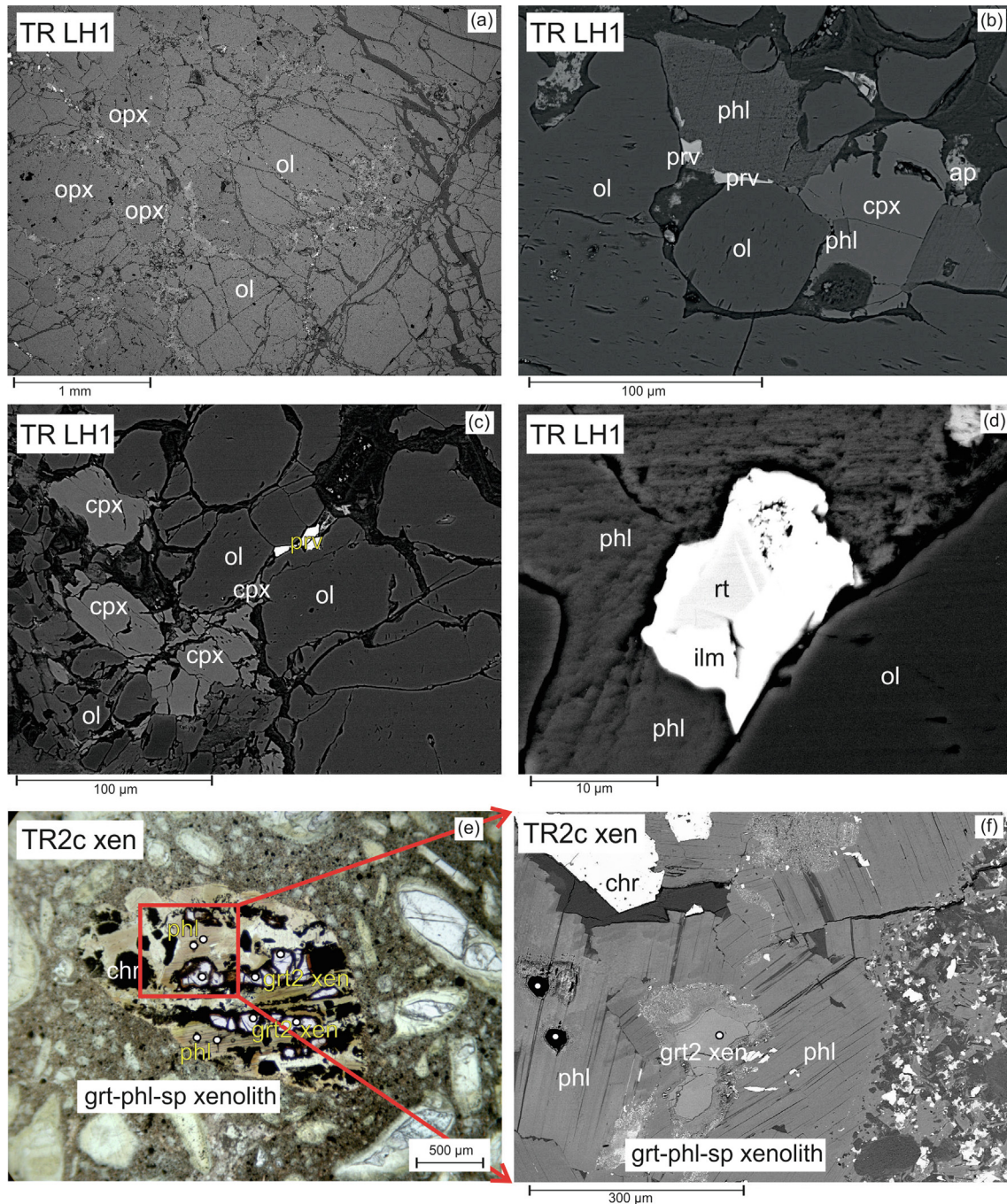


Fig. 3. Back-scattered electron images and thin section photomicrographs illustrating the main petrographic features of the lherzolite TR LH1 (a–d) and garnet-phlogopite-spinel xenolith TR2c (e–f). Abbreviations used: ap, apatite; chr, chromite; cpx, clinopyroxene; grt, garnet; ilm, ilmenite; ol, olivine; opx, orthopyroxene; phl, phlogopite; prv, perovskite; rt, rutile (Warr, 2021).

and nearly flat HREE (about 10 times chondrite), relatively fractionated MREE ($Sm_N/Yb_N = 0.03–0.29$), highly fractionated and very low LREE ($La_N = 0.003–0.05$; Fig. 8b). The TR8 grt1 ($Sm_N/Yb_N = 0.59–1.28$), TR8 grt3 ($Sm_N/Yb_N = 0.66–1.21$), and TR9 grt ($Sm_N/Yb_N = 0.77–0.92$) have sinusoidal patterns, that are slightly convex upward in the MREE region and with positive slope in the HREE region (Fig. 8a). TR8 grt2 has a sinusoidal pattern but with the lowest MREE and HREE contents ($Sm_N/Yb_N = 0.67–1.28$), about 1–3 times chondrite, compared to the previous four garnets, which are enriched 7–10 times chondrite (Fig. 8a,b). A different pattern was observed in the garnet TR11 (Fig. 8). It has a spoon-like pat-

tern, upward convexity, heavily depleted in MHREE (0.1–0.3 times chondrite; $Sm_N/Yb_N = 0.05–0.16$), with La_N (0.16–0.19) lower than Yb_N (0.34–0.54) and high La_N/Yb_N (0.77–0.92).

Both sinusoidal REE- and HREE-enriched steadily fractionated patterns are, respectively, typical of garnet-facies lherzolites and magmatic garnet-bearing cumulates from basaltic melts [Vitim, Siberia (Glaser et al., 1999; Ionov et al., 2005a); Kakanui, New Zealand (Zack et al., 1997; Fulmer et al., 2010); Kaapval Craton, South Africa (Grégoire et al., 2003)], and are commonly observed in metasomatized mantle peridotites (cf. Ziberna et al., 2013a; le Roex and Class, 2016). The highly fractionated REE patterns observed for the

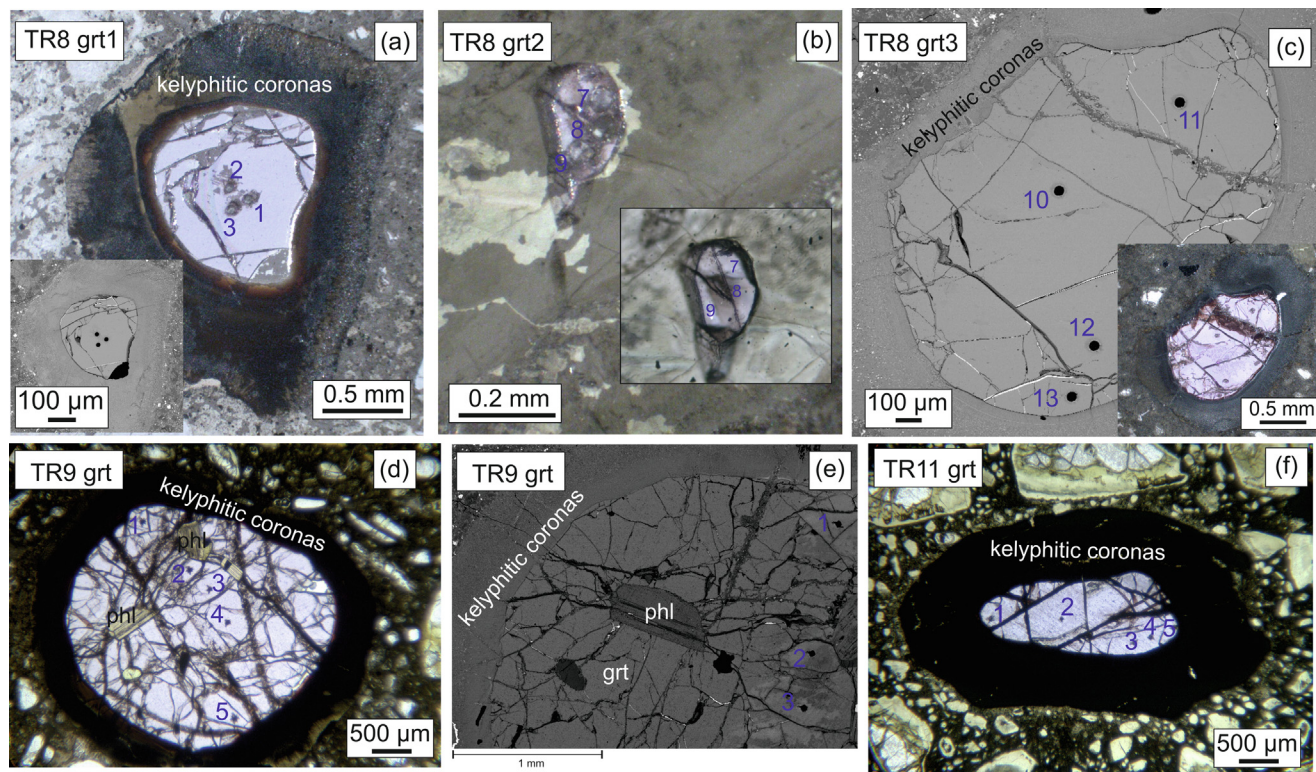


Fig. 4. Back-scattered electron images and thin section photomicrographs of analyzed garnet xenocrysts: (a) TR8 grt1, (b) TR8 grt2, (c) TR8 grt3, (d-e) TR9 grt, and (f) TR11 grt.

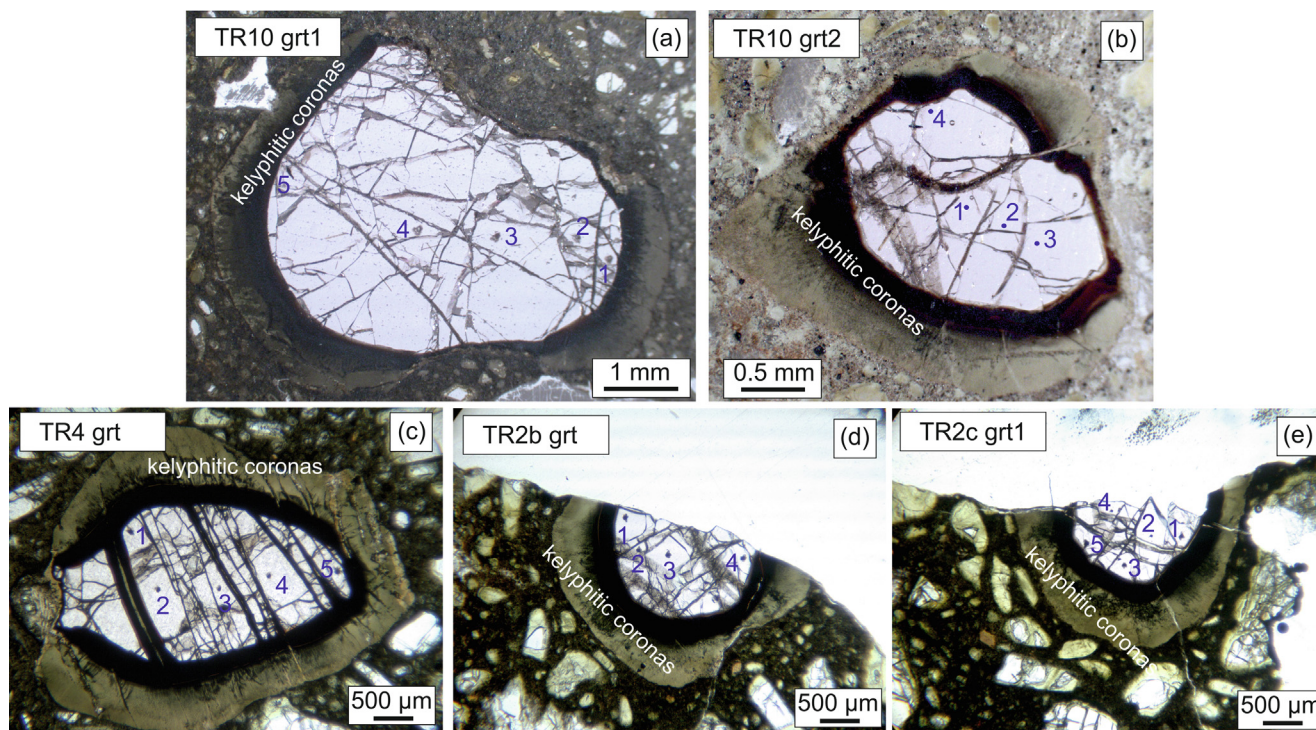


Fig. 5. Back-scattered electron images and thin section photomicrographs of analyzed garnet xenocrysts: (a) TR10 grt1, (b) TR10 grt2, (c) TR4 grt, (d) TR2b grt, and (e) TR2c grt1.

Três Ranchos garnets are consistent with garnets typically found in SCLM cratons (e.g., Siberian and Kaapval Cratons; Grégoire et al., 2003; Ziberna et al., 2013a,b; Tappe et al., 2021).

Compared to our Três Ranchos garnets, the Osvaldo França 1 garnets have a wide variability in the major and trace element compositions, but no analogue of the trace element patterns of

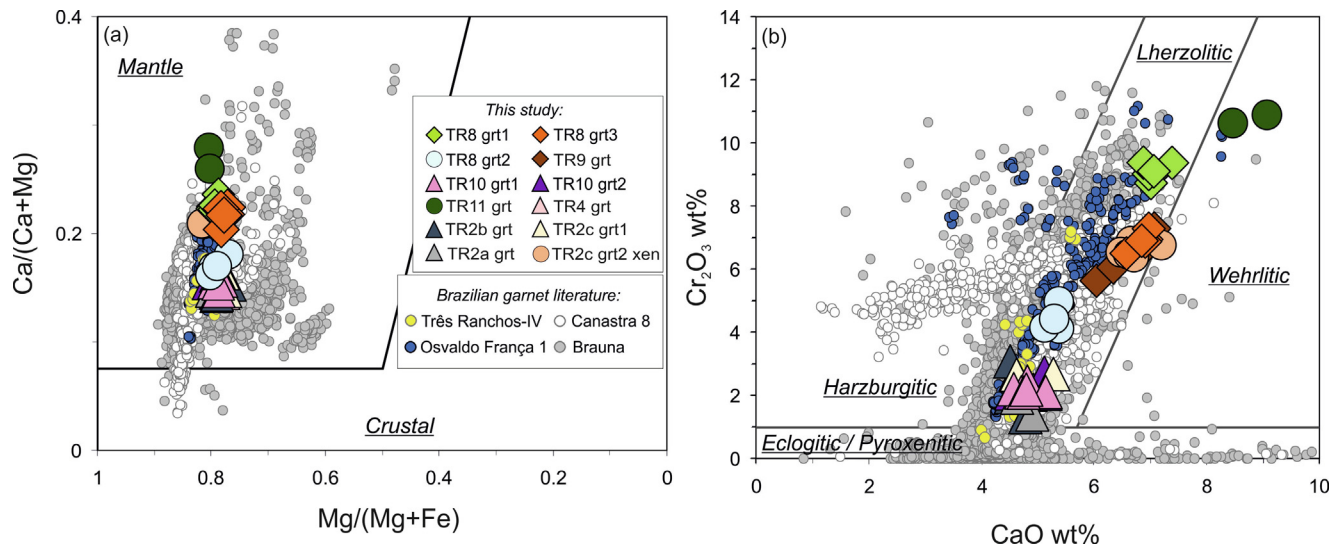


Fig. 6. Chemical characteristics of analyzed garnet xenocrysts using the following discriminant diagrams: (a) $\text{Mg}/(\text{Mg} + \text{Fe})$ vs. $\text{Ca}/(\text{Ca} + \text{Mg})$ and (b) CaO vs. Cr_2O_3 (Schulze, 2003; Grütter et al., 2004). Literature data are from Donatti-Filho et al. (2013), Hill et al. (2015), and Carvalho et al., (2022a).

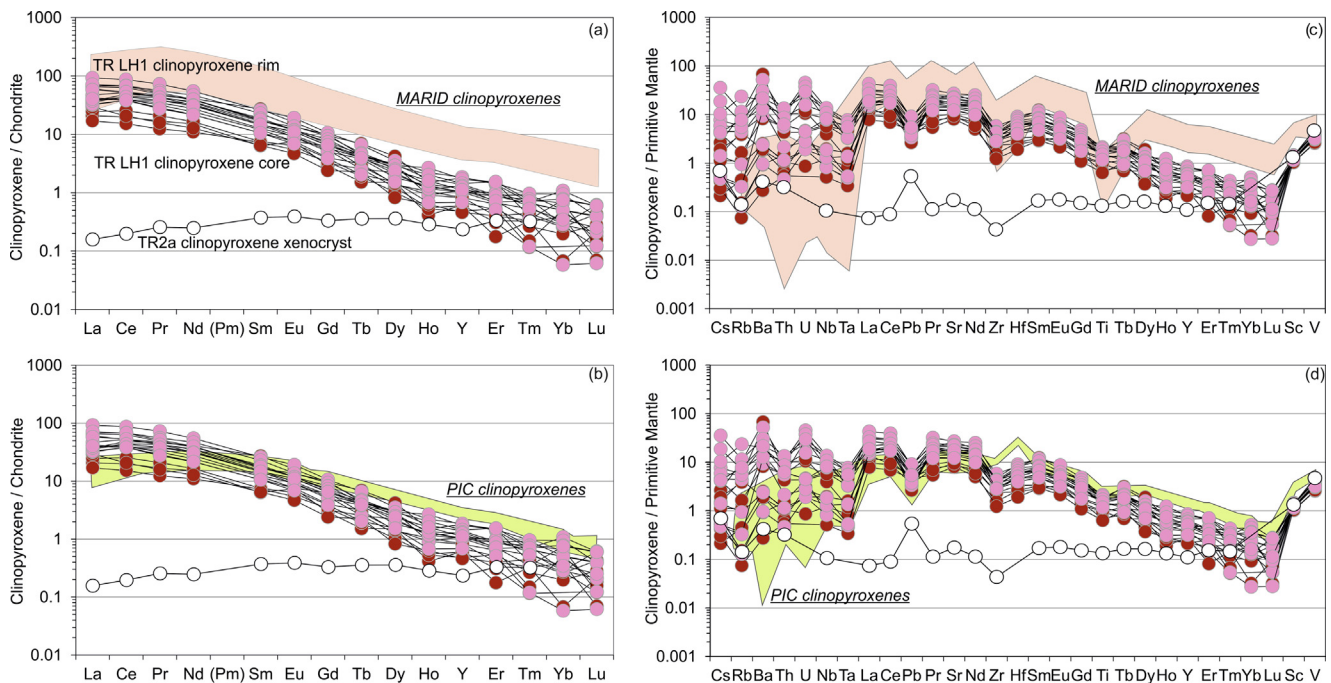


Fig. 7. Chondrite-normalized REE and multi-element patterns for TR2a clinopyroxene xenocryst and TR LH1 clinopyroxenes compared to (a,c) MARID (Mica-Amphibole-Rutile-Ilmenite-Diopside) and (b,d) PIC (Phlogopite-Ilmenite-Clinopyroxene) clinopyroxene fields (Fitzpayne et al., 2018). Normalization values are taken from Anders and Grevesse (1989) and Lyubetskaya and Korenaga (2007).

TR11 garnet xenocryst and TR2c grt2 in the grt-phl-sp xenolith have been documented (Figs. 6 and 8; Carvalho et al., 2022a). There is only a similarity in the HREE-enriched, steadily fractionated REE patterns of TR10 grt1, TR10 grt2, TR4 grt, TR2b grt and TR2c grt1 to those of lherzolite-1 [low Cr_2O_3 (1.7–6.9 wt%) and a homogeneous REE pattern; Carvalho et al., 2022a] and the sinusoidal patterns of TR8 grt2 to those of lherzolite-2 and especially to those of wehrlite-2 [both characterized by high Cr_2O_3 (7.4–11.2 wt%) and a sinusoidal pattern with a significant hump in the middle REE; Carvalho et al., 2022a]. In the primitive mantle-normalized incompatible element diagram (Fig. 8d–f), Pb, U, Hf and Zr are close to 1 in both Três Ranchos and Osvaldo França 1 garnets.

4.3. Temperature and pressure estimates

The estimated T, P, and depth of provenance of the studied samples are summarized in Table 2. True P–T estimates for harzburgite TR2a, lherzolite TR11, garnet-phlogopite-spinel xenolith TR2c and clinopyroxene xenocryst TR2a fall along a model conductive geotherm calculated for a surface heat flow of 40 mW/m² (Hasterok and Chapman, 2011; Fig. 9; Table 2).

Four of the garnet xenocrysts (TR11 grt, TR8 grt1, and TR8 grt3) also fall very close to this geotherm, suggesting equilibrium with spinel. This is compatible with the wide stability range of spinel + garnet in mantle peridotites (Ziberna et al., 2013a).

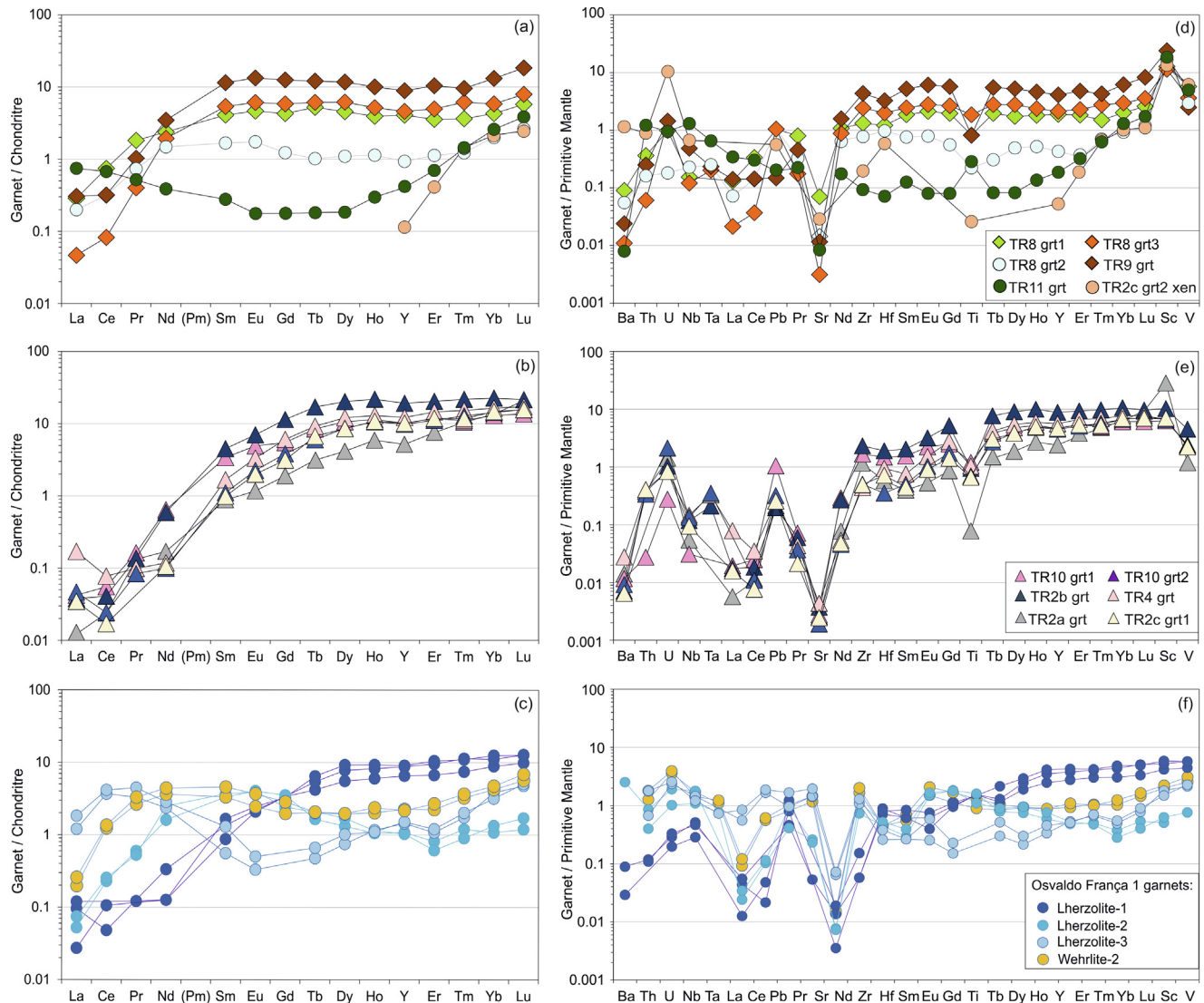


Fig. 8. Chondrite-normalized REE and multi-element patterns for mean values of Três Ranchos garnet xenocrysts (a,b,d,e) compared to the main representative garnets (lherzolite-1, lherzolite-2, wehrilite-2, and lherzolite-3) of Osvaldo França 1 (Carvalho et al., 2022a). Normalization values are taken from Anders and Grevesse (1989) and Lyubetskaya and Korenaga (2007).

The minimum P estimates for the remaining six garnet xenocrysts (TR8 grt2, TR10 grt1, TR10 grt2, TR2b grt, TR2c grt1, TR4 grt) are much lower than the geotherm, which denotes the absence of spinel in the original mineral assemblages. After projecting all garnet xenocryst temperatures onto the geotherm, the P–T range covered by all studied samples is ca. 3–5 GPa and 800–1200 °C (Fig. 9; Table 2).

Most of the garnet xenocrysts and the clinopyroxene xenocryst were derived from a restricted P–T range centered at about 3.2 GPa and 830 °C. The remaining two garnet xenocrysts, the garnet-phlogopite-spinel xenolith and the harzburgite xenoliths record slightly hotter and deeper conditions of 3.3–3.9 GPa and 900–940 °C. All these samples fall within the graphite stability field. The lherzolite xenolith records much higher P and T conditions (about 5 GPa and 1200 °C) and falls well within the diamond stability field. Overall, the calculated P values correspond to a depth interval of ~ 100–160 km (Table 2). These new data thus extend the pressure range previously estimated by Coldebella et al., (2020; P = ~1.8–3.4 GPa) to higher values. On a regional scale, the estimated pressures for garnets in the literature are ~ 1–4 GPa at Canastra 8 (Hill et al., 2015), and up to 5 GPa at Brauna

(Donatti-Filho et al., 2013). An estimated P range of 1.8–3.6 GPa has also been reported for garnet in the Vargem 1, Grota do Cedro, Abel Régis and Romaria kimberlites (Carvalho et al., 2022a and references therein). These P estimates, however, should be considered as minimum estimates since equilibrium with spinel is not documented. In the case of Osvaldo França 1, the kimberlite-borne garnet xenocrysts indicate equilibration temperatures of 811–875 °C (Carvalho et al., 2022a). The envelope of maximum P at any given T allows us to estimate a geotherm at the time of eruption corresponding to a ca. 35–36 mW/m² model conductive geotherm (Fig. 9). When the garnet data for Osvaldo França 1 are projected onto the local geotherm, a P range of 3.9 to 4.4 GPa is estimated (Suppl. Table 10).

4.4 Equilibrium melt calculation in garnet and clinopyroxene xenocrysts, and clinopyroxenes in lherzolite xenolith

We calculated the concentration of several incompatible trace elements (e.g., Ti, Sr, Y, Zr, Nb, Hf, La, Ce, Nd, Sm, Eu, Dy, Er, Yb, and Lu) in the equilibrium melt composition using the concentration of these elements in the garnet xenocrysts and clinopyroxenes

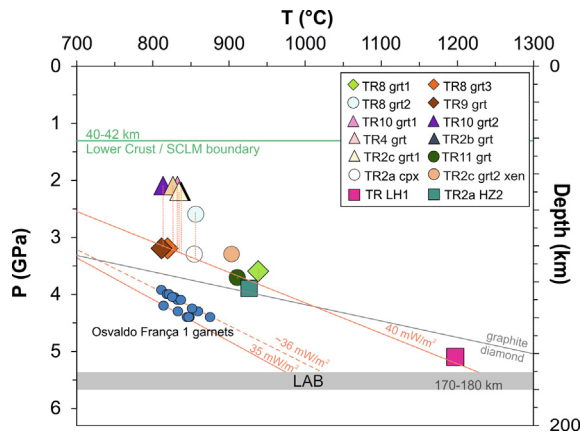


Fig. 9. Temperatures, pressures, and depths for the studied samples. Temperatures (Carvalho et al., 2022a) and geotherm-projected pressures (Suppl. Table 10) for Osvaldo França 1 are shown for comparison. Conductive model geotherms (light orange) from 35 to 40 mW/m² are from Hasterok and Chapman (2011). The diamond/graphite equilibrium is from Day (2012). The lower crust/SCLM boundary (green) is from Alton et al. (2022) and Assumpção et al. (2004). The LAB is from Fig. 9 proposed in Rocha et al. (2019) and obtained from Priestley et al. (2018) through the study of surface-wave tomography inversions with petrological constraints. (For interpretation of the references to colour in this figure legend, the reader is referred to the web version of this article.)

in the Iherzolite xenolith TR LH1, and the partitions coefficients experimentally defined by Johnson (1998) for clinopyroxene/liquid and garnet/liquid. The obtained results are reported in Suppl. Table 11 and Fig. 10. The calculated trace element concentrations of equilibrium melt composition (C_{liquid}) from clinopyroxene core compositions matches those calculated from TR8 grt1 xenocryst. They also approach the fractionation of the host kimberlite (and that of a typical kamafugite from Presidente Olegário; Guarino et al., 2013), suggesting equilibrium with an ultra-alkaline and carbonated silicate melt of similar geochemical affinity.

A very similar depleted trace element concentration is found for the equilibrium melt composition (C_{liquid}) calculated for TR11 garnet, TR2c garnet in the grt-phl-sp xenolith, and TR2a clinopyroxene xenocryst. Differently, the equilibrium melt composition calculated for TR8 grt3, TR8 grt2, TR9 grt, TR10 grt1, TR10 grt2, TR4 grt, TR2c grt1, TR2b grt1 and TR2a grt1 have a lesser enrichment in Nb, La, Ce, and Sr, with some differences in the fractionation trend defined by other elements.

5. Discussion

The type and composition of the garnet xenocrysts, together with the petrographic features and mineral assemblages of the peridotite xenoliths, as well as the uncontaminated nature of the host kimberlite, provide useful information about the geothermal state of the SCLM beneath the APIP and constraints on the stabilization processes and evolution of the Brazilian subcontinental lithospheric mantle at the local and regional scales.

5.1. Constraints on the mantle source of APIP kimberlites

Guarino et al. (2013) proposed that the APIP kimberlite and kamafugite magmatism was produced by low degrees of partial melting of an old, heterogeneous, metasomatized and oxidized/carbonated (C–H-bearing) garnet-facies phlogopite-rich Iherzolite, enriched in incompatible elements, which did not undergo any interaction with the convective mantle or with any hypothetical melts derived from a Trindade mantle plume. Typically, the source of kimberlites is considered to be located at the lithosphere-

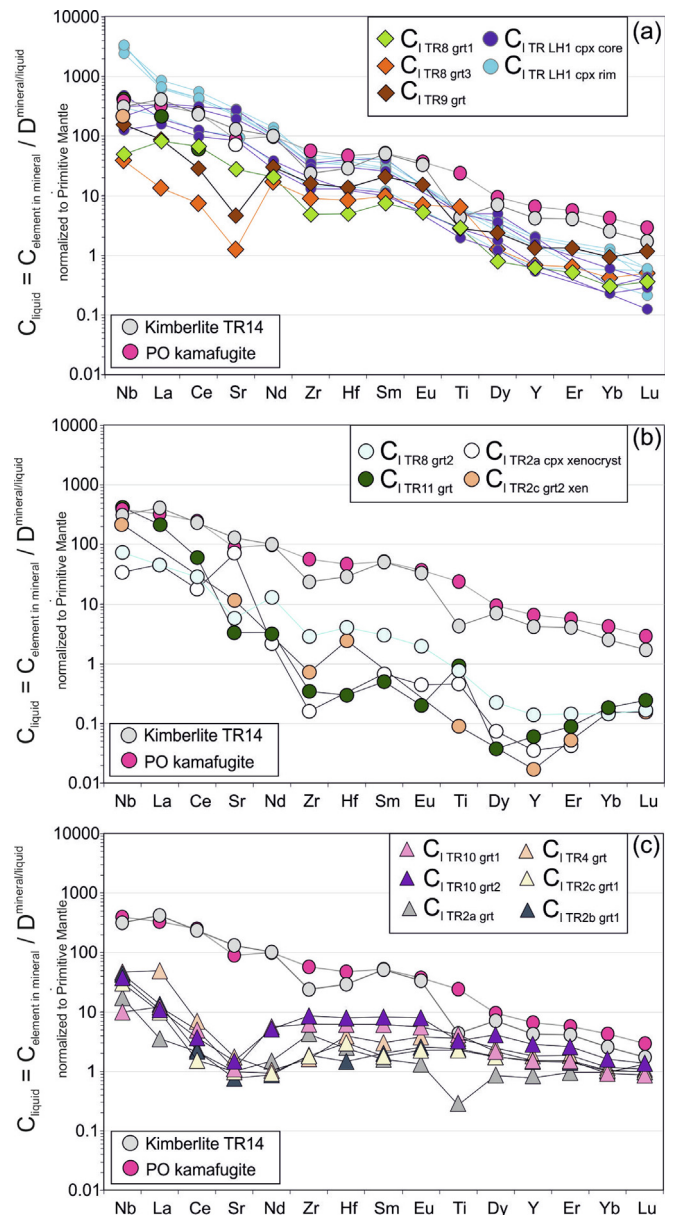


Fig. 10. Results of the numerical simulation of the equilibrium melt composition (C_{liquid}) calculated for (a) TR8 grt1, TR8 grt3, and TR9 grt, compared with the equilibrium melt composition (C_{liquid}) calculated for the main clinopyroxene cores and rims analyzed in the Iherzolite xenolith TR LH1, (b) TR8 grt2, TR11 grt, TR2c grt2 in grt-phl-sp xenolith (xen) and TR2a clinopyroxene (cpx) xenocrysts, and (c) TR10 grt1, TR10 grt2, TR4 grt, TR2c grt1, TR2b grt1, and TR2a grt. In these diagrams, the Três Ranchos kimberlite (TR14) and the Presidente Olegário (PO) kamafugite (Melluso et al., 2008) are shown. Normalization values are taken from Lyubetskaya and Korenaga (2007).

asthenosphere boundary (LAB) (e.g., Donatti-Filho et al., 2013; Ferreira et al., 2022 and references therein), which is also supported by new tungsten-182 isotope data for all kimberlites in sub-Saharan Africa through time (Tappe et al., 2020). The depth of the mantle source of the Três Ranchos kimberlite is probably at 170–180 km (Rocha et al., 2019), similar to that typically estimated for Upper Permian-Mesozoic kimberlites erupted within the Amazonian and São Francisco Cratons (e.g., Gervasoni et al., 2022; Ferreira et al., 2022 and references therein).

This type of mantle source typically experienced re-fertilization processes as testified by its pronounced enrichment in volatiles and highly incompatible elements. Carvalho et al., (2022b)

proposed that the re-fertilization processes in the APIP lithosphere occurred in the Proterozoic. [Rodrigues et al. \(2023\)](#), based on the high clinopyroxene/orthopyroxene ratios of some spinel lherzolite xenoliths on the Catalão kimberlites (near Três Ranchos) and on the typical metasomatic trace-element signatures of the clinopyroxene xenocrysts, suggest a pervasive re-fertilization of the cratonic APIP lithosphere where the typically depleted peridotites of cratonic regions have been replaced by a pyroxene-rich lithology. Consistently, [Ferreira et al. \(2022\)](#) suggest that the Mesozoic alkaline and tholeiitic magmatism in western Brazil, involving the APIP, is related to metasomatized mantle sources enriched in CO_2 , H_2O , and incompatible elements produced by subduction processes since the Neoproterozoic, probably related to dehydration processes of carbonated oceanic crusts and heterogeneous subducted sediments or older collisional events (see also [Sun and Dasgupta, 2020](#)). Indirect evidence for these subduction processes is associated with the eclogitic garnet and clinopyroxene inclusions in diamonds from the APIP region ([Carvalho et al., 2022b](#)). Similarly, the diamond-bearing Brauna kimberlite has been interpreted as the result of partial melting (<1%) of metasomatized mantle lithosphere at the base of the São Francisco craton with minor asthenospheric mantle input. Even, the similar isotopic composition of the oldest Brauna kimberlites (~642 Ma; initial ϵ_{Nd} values from -5.8 to -8.1 and $^{87}\text{Sr}/^{86}\text{Sr}_i = 0.7045\text{--}0.7063$; [Donatti-Filho et al., 2013](#)) and the youngest APIP rocks (~91–78 Ma; initial ϵ_{Nd} values of -3.9 to -6.6 and $^{87}\text{Sr}/^{86}\text{Sr}_i = 0.7043\text{--}0.7069$; [Guarino et al., 2013](#)) suggest a similar source in the Brazilian SCLM, which produced two similar (proto)kimberlite melts that are homogeneous over a large span of time and space. This is supported by the model of global kimberlite volcanism proposed by [Tappe et al. \(2018\)](#). A key element of this model is that kimberlite melts are ubiquitous in the LAB region, and that surface kimberlite magma eruption events are largely dependent on suitable tectonic triggers.

5.2. Thermal structure of the Brazilian SCLM

During the rapid ascent of the Três Ranchos (proto)kimberlite melt through the SCLM, garnet xenocrysts and peridotite xenoliths were entrained across a depth interval of 160–100 km, in a pressure interval of 5–3 GPa, associated with a temperature decrease from ~1200 to 800 °C ([Fig. 9](#); [Table 2](#)). Geothermobarometric estimates for the entrained materials fall on a typical cratonic conductive geotherm calculated for a 40 mW/m² surface heat flow ([Fig. 9](#); [Hasterok and Chapman, 2011](#)). This heat flow through the Três Ranchos SCLM during the Cretaceous is slightly higher than that recorded at Canastra 8 (~35 mW/m²; [Hill et al., 2015](#)) and Osvaldo França 1 (~35–36 mW/m², this work), but similar to that reported for other diamondiferous kimberlites in the region (~39 mW/m²; [Carvalho et al., 2022b](#)).

All the information reviewed here indicates that the subcontinental lithospheric mantles of Três Ranchos, Canastra 8, and Osvaldo França 1 are all representative of the subcratonic southwestern margin of the São Francisco Craton, entirely within the terrain attributed to the São Francisco Palecontinent ([Rocha et al., 2019](#)). Geophysical data suggest that the SCLM in these areas is significantly thinner than in the more inner portions of the São Francisco and Amazonian Cratons, where the base of the lithosphere is located at depths > 200 km ([Rocha et al., 2019](#); [Ferreira et al., 2022](#)). Present-day SCLM thickness is similar between the Três Ranchos (~170–180 km; [Rocha et al., 2019](#)) and Osvaldo França 1 (~181 km; [Priestley et al., 2018](#)). The variability in heat flow is justified by recent seismic tomography data (see [Fig. 3b](#) in [Rocha et al., 2019](#)). These data show a large high-velocity anomaly in the region of the São Francisco cratonic margin, suggesting a stable and cool structure, typical of cratonic regions, and a transition to low-velocity anomalies when approaching mobile belt

areas such as the APIP (Brasília Mobile Belt). Taken together, our data would support a scenario in which the slightly hotter Três Ranchos Cretaceous SCLM is located within the APIP and is involved in the early geodynamic evolution of the Brasília Mobile Belt; while the slightly cooler Osvaldo França 1 lithospheric column lies in a realm that better preserves the original physical-chemical features of the São Francisco Craton. This hypothesis highlights the possibility of having slight variations in heat flow on a relatively short space and time scales, depending on geodynamic evolution and deep lithospheric processes.

5.3. Chemical zoning of the Brazilian SCLM

It is a generally accepted that the lithosphere beneath cratonic areas is composed of depleted peridotites [i.e., mainly harzburgites and dunites with subordinate orthopyroxenite], which were produced by large to extreme degrees of partial melting in the Archean times (e.g., [Bernstein et al., 2007](#); [Aulbach et al., 2017](#); [Ionov et al., 2020](#)). These are more buoyant than the rest of the mantle and stable for billions of years. The ancient history of chemical depletion is also revealed by the local preservation of high $^{176}\text{Hf}/^{177}\text{Hf}$ and $^{143}\text{Nd}/^{144}\text{Nd}$ isotopic ratios in xenoliths from basalts and kimberlites in Precambrian terrains and Archean cratons (e.g., [Lee et al., 2011](#)), which are often associated with ancient unradiogenic $^{187}\text{Os}/^{188}\text{Os}$ isotopic compositions that record ancient depletion ages ([Reisberg and Lorand, 1995](#); [Shirey and Walker, 1998](#)). Furthermore, extremely variable Nd-Hf isotopic ratios characterize these cratonic peridotites, suggesting that the long-term preservation of depletion signatures may be locally overprinted by more recent metasomatic events (e.g., [Tilhac et al., 2022](#)). Geophysical studies indicate that the core of the cratons is composed of much more depleted peridotites than reconstructed from xenoliths brought to the surface by basaltic/kimberlitic melts of deep origin, which have typically mantle columns significantly more affected by re-fertilization processes ([Artemieva et al., 2019](#)).

According to the garnet compositions, the SCLM below the Três Ranchos kimberlite is mainly composed of lherzolite ([Fig. 6b](#)), indicating extensive re-fertilization induced by pervasive melt migration (e.g., [Griffin et al., 1996](#); [Ziberna et al., 2013a,b](#)). The extent of re-fertilization is not homogeneous in the SCLM below the APIP region. For example, the mantle column appears to be less fertile beneath the Canastra 8 kimberlite, located in the southernmost part of the APIP, where harzburgitic garnet xenocrysts are abundant. The composition of the garnet xenocrysts in the Osvaldo França kimberlite area, located at the boundary between the APIP and the São Francisco Craton, is dominated by the occurrence of lherzolite and minor harzburgitic and wehrilitic ones. Harzburgite is also present, but subordinate, below the Brauna kimberlite area (northeastern sector of the São Francisco Craton), where lherzolite and pyroxenite are abundant.

Complex compositional zoning in the deep Brazilian SCLM beneath the Três Ranchos kimberlite in the APIP region is revealed by variations in the major and trace element compositions of garnet and clinopyroxene xenocrysts, as well as of peridotite xenoliths.

In particular, extensive metasomatic processes occurring at a depth of ca. 160 km are revealed by the chemical and petrographic characteristics of the lherzolite xenolith TR LH1. Petrographic evidence indicates that the peridotite matrix was originally a harzburgite dominated by large olivine and minor orthopyroxene. Clinopyroxene was added as rounded crystals replacing olivine, pointing to extensive interaction of the peridotite matrix with a silicate alkaline melt. The similarity of the trace element composition between the liquid calculated in equilibrium with the clinopyroxenes and ultra-alkaline melts ([Fig. 10](#)) highlights a complete geochemical reset of the TR LH1 peridotite, as is typically shown by

peridotites experiencing large time-integrated melt-rock during porous flow melt percolation (e.g., [Piccardo et al., 2007](#) and references therein).

A second melt percolation event resulted in interstitial segregation of the fine-grained mineral assemblage consisting of phlogopite, perovskite, clinopyroxene, rutile, and ilmenite, with the partial recrystallization/replacement of olivines and pyroxenes, which became partially cloudy due to the widespread segregation of microscopic inclusions. The second melt injection was apparently short-lived, but there is no petrographic evidence as to whether it was related to the host kimberlite during the ascent to the surface or to earlier percolation processes. The interstitial the fine-grained mineral assemblage testifies that the second injected melt was strongly silica-undersaturated and of ultra-alkaline affinity ([Fig. 3a-d](#)). It was also characterized by high oxygen fugacity activity, as evidenced by the presence of Fe^{3+} in the tetrahedral site of phlogopites ([Guarino and Brigatti, 2018](#) and references therein).

Large clinopyroxenes show complex Al and Cr variations, as well as Fe enrichments in the rim, which are apparently the result of the interaction with the late injected melt. Nevertheless, the very similar fractionation exhibited by both the core and the rim of the clinopyroxene from Nd to V was probably acquired during the first percolation event ([Fig. 7c,d](#)). Conversely, the random enrichments of highly incompatible elements (La and Ce, LILE, U, Th) may be ascribed to the presence of melt inclusion entrapment and solid-state diffusion that occurred during the second melt pulse ([Fig. 7c,d](#)).

The large $(\text{LREE}, \text{Sr})_{\text{N}}/\text{HREE}_{\text{N}}$ and $\text{REE}_{\text{N}}/\text{HFSE}_{\text{N}}^{4+}$ ratios in clinopyroxene cores for the Iherzolite xenolith TR LH1, associated with $\text{Sc}_{\text{N}} < \text{V}_{\text{N}}$ ([Fig. 7](#)), suggest the development of a pervasive metasomatism driven by a melt extremely enriched in highly incompatible elements at garnet-facies mantle depths (see [Figs. 10-12](#); [Nimis et al., 2009](#)), consistent with the high estimated, high equilibrium T and P (1200 °C and 5 GPa; [Table 2](#)).

According to the Crank's equation ([Crank, 1979](#)) and the high-T (1200 °C) ambient conditions, the preservation of core-rim zoning indicates that the melt injections developed over a time span of a few hundred to tens of thousands of years prior to the surface emplacement of the TR LH1 sample (see also [Ionov et al., 2002](#); [Ziberna et al., 2013a](#); [Jollands et al., 2018](#)), presumably within the framework of the magmatic cycle that produced the host (proto)kimberlite melt.

An overall MARID affinity ([Fitzpayne et al., 2018](#)) of the metasomatic melts and the host-kimberlite is supported by the large $\text{REE}/\text{HFSE}^{4+}$ ratios presented by Iherzolite clinopyroxenes, associated

with the presence of clinopyroxene, phlogopite, rutile and ilmenite as newly formed minerals in Iherzolite, and potassic richterite + phlogopite in the microcrystalline silicate-carbonate groundmass of the Três Ranchos kimberlite.

5.3.1. A metasomatized (\pm phlogopite) peridotite layer

A layer containing metasomatized (\pm phlogopite) peridotite [class L19 according to the CARP (Cluster Analysis by Regressive Partitioning) classification tree in [Griffin et al., 2002](#)] at depths between 124 and 105 km (3.1–3.9 GPa and 811–940 °C) is identified by the thermobarometric estimates and chemical compositions of three garnet xenocrysts (TR8 grt1, TR8 grt3, and TR9 grt).

The slightly sinusoidal REE patterns of TR8 grt1 are common in cratonic SCLM and are generally considered to be the result of interactions between refractory peridotite and silicate melts ([Grégoire et al., 2002](#); see also Group B and secondary garnets in [Ziberna et al., 2013a](#)). Consistently, the Y, Zr, and Ti contents of TR8 grt1 are at the lower end of the garnet compositional field attributed to silicate melt metasomatism ([Fig. 11](#)). The melt calculated to be in equilibrium with TR8 grt1 has trace element concentrations and fractionations approaching those of the Três Ranchos kimberlite (Suppl. [Fig. 6](#)). This suggests that the SCLM sector documented by TR8 grt1 ($T = 938$ °C; $P = 3.8$ GPa; depth = 120 km) has undergone a strong geochemical reset, approaching the equilibrium with a metasomatic agent that may have a carbonated and ultra-alkaline affinity, such as the (proto)kimberlite melt. Similar conclusions based on equilibrium melt calculations were reached by [Tappe et al., \(2021](#) and references therein) for the Premier kimberlite pipe (Kaaopval Craton), where metasomatic garnet porphyroclasts were interpreted to be derived by the interaction with carbonated silicate melts such as kimberlitic melts near the lithosphere-asthenosphere boundary at depths between 220 and 150 km.

Within this intermediate sector, at a depth of 100 km, the presence of phlogopite metasomatism is documented by garnet TR9 ($T = 811$ °C; $P = 3.1$ GPa; [Fig. 11a](#)), which contains small phlogopite crystals ([Fig. 4d-e](#)) and Zr and Ti contents typical of such metasomatism ([Fig. 11a](#)). However, at the same depth and at similar temperature and pressure, TR8 grt3 ($T = 819$ °C; $P = 3.2$ GPa) was identified. The Zr, Y and Ti contents of this garnet document a melt metasomatism ([Fig. 11](#)). The melts calculated to be in equilibrium with TR9 grt and TR8 grt3 have similar patterns, markedly depleted in La, Ce and Sr, and for other elements approaching the melt calculated to be in equilibrium with TR8 grt1 pattern.

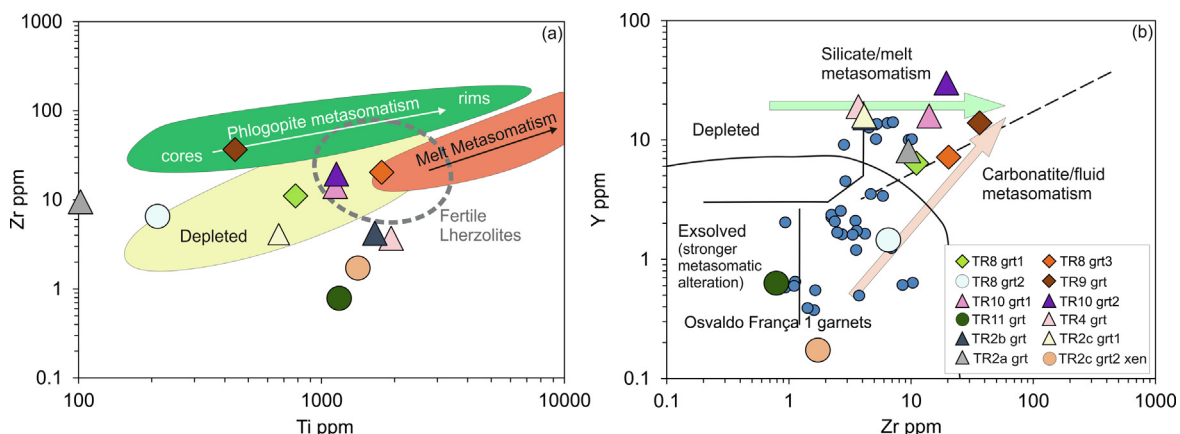


Fig. 11. Diagrams of (a) Zr vs. Ti ([Griffin et al., 2002](#)) and (c) Y vs. Zr ([Ragozin et al., 2021](#) and references therein) used for the analyzed garnet xenocrysts. The Oswaldo França 1 data are reported to comparison ([Carvalho et al., 2022a](#)).

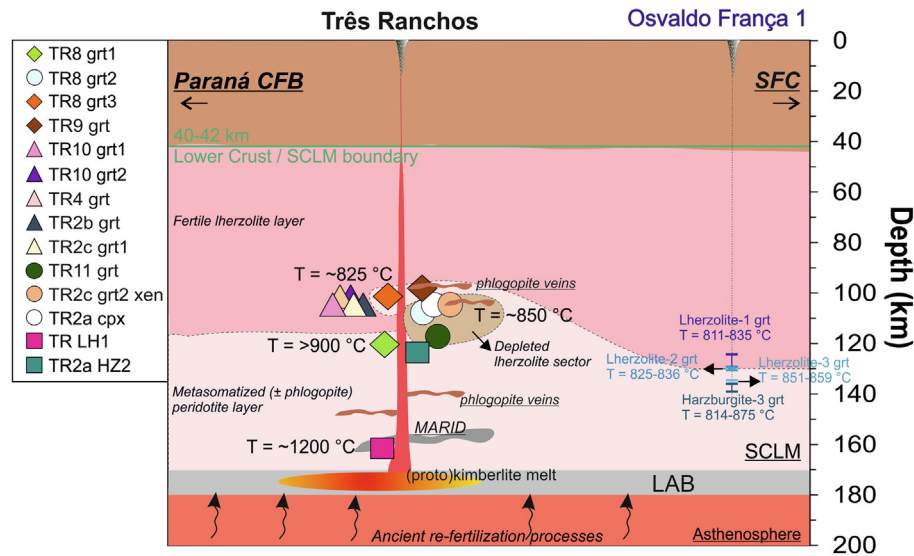


Fig. 12. Representative schematic model of thermal and chemical zoning of Brazilian SCLM defined in this study. The LAB is from Fig. 9, proposed in Rocha et al. (2019), and obtained from Priestley et al. (2018) through the study of surface-wave tomography inversions with petrological constraints. Abbreviations: Paraná CFB, Paraná continental flood basalts, and SFC, São Francisco Craton.

5.3.2. A depleted lherzolite sector

The strongly depleted REE patterns of TR11 grt and TR2c grt2 in the garnet-phlogopite-spinel xenolith (900–910 °C, 3.4–3.7 GPa, and 110–115 km depth), and the similarity of their equilibrium melt patterns (Fig. 10), suggest the presence of a depleted lherzolite sector (CARP-L3 class; Griffin et al., 2002). The similarity between the equilibrium melt pattern calculated for these garnets and that for the TR2a clinopyroxene xenocryst coming from a similar depth (3.3 GPa) suggests that this clinopyroxene is derived from the same depleted lherzolite sector (Figs. 9 and 12).

The presence of this depleted sector is also confirmed by TR8 grt2 ($T = 850$ °C; $P = 3.4$ GPa and 110 km depth), which again falls in the CARP-L3 class (Griffin et al., 2002). This garnet has a strongly sinusoidal REE pattern. The very low MREE and HREE contents, about 1–3 times the chondritic values, associated with the lowest Y, Ti, and Zr concentrations (Fig. 11) found in Três Ranchos garnets, suggest a derivation from a strongly depleted peridotite matrix produced by high degrees of melt extraction. Conversely, the phlogopite overgrown in TR2c grt2 and the relatively high LREE concentrations are indicative of metasomatic overprinting. Similar concentrations and fractionations can result from fluid-related metasomatism (Fig. 11) or, alternatively, they may represent transient geochemical compositions imparted by differentiated silicate melts that evolved through chromatographic-type chemical exchange with a depleted ambient peridotite (Ziberna et al., 2013a; le Roex and Class, 2016). Similarly, garnets with sinusoidal to spoon shaped REE patterns have also been documented in the mantle column beneath Osvaldo França 1. These garnets have been interpreted to reflect geochemical gradients developed in depleted peridotites during a unique re-fertilization event related to the injection of (i) a silicate melt with subalkaline/tholeiitic geochemical affinity as a consequence of recycling of oceanic crust by Neoproterozoic subduction, and (ii) a silicate melt originating from an enriched, deep mantle source ascending after slab tearing (Carvalho et al., 2022a,b).

Nevertheless, the reconstruction of the geochemical affinity of primitive liquids in the presence of transient compositions produced by highly evolved differentiated melts is very difficult in the absence of reference compositions that allow a clear definition of the fractionation trends. In this context, it cannot be excluded

that the sinusoidal pattern of the TR8 grt2 is related to fractionation via interaction of a depleted mantle sector with the same ultra-alkaline liquid responsible for the metasomatism of the deepest sectors of the Três Ranchos mantle column.

5.4. On the nature of the fertile lherzolite layer of the Brazilian SCLM

A fertile lherzolite layer (CARP-L9 class; Griffin et al., 2002) at a depth of ca. 100 km is documented by most of the analyzed garnet xenocrysts (TR10 grt1, TR10 grt2, TR4 grt, TR2b grt, and TR2c grt1) showing both a LREE depletion and a HREE enrichment (Fig. 8b,e). All these garnets are derived from a relatively shallow P-T interval at about 3.2 GPa and 825 °C.

These garnets have the typical linearly fractionated, LREE-depleted, and HREE-enriched pattern of kimberlite-borne Cr-poor garnet megacrysts worldwide (Suppl. Fig. 6; see Group A garnets in Ziberna et al., 2013b; updated reference list in Carvalho et al., 2022a). Their major and trace element compositions mimic those of the lherzolite-1 garnet group from the Osvaldo França 1 kimberlite (Fig. 8; Carvalho et al., 2022a). Their Y, Zr, and Ti contents are at the lower end of the compositional field of garnet produced by silicate melt metasomatism and are close to the field of depleted garnets (Fig. 11). Accordingly, such compositions are generally interpreted to reflect silicate melt metasomatism (e.g., Stachel et al., 1998; Stachel and Harris, 2008; Agashev et al., 2013; Ziberna et al., 2013b; Shu and Brey, 2015; le Roex and Class, 2016; Shchukina et al., 2017, 2019; Dymshits et al., 2020; Shaikh et al., 2020).

The melts calculated to be in equilibrium with these garnets (Fig. 10b) suggest that the putative metasomatic/magmatic silicate agent must be significantly less enriched in LREE and more enriched in HREE than ultra-alkaline melts, such as APIP kimberlites and kamafugites. On the other hand, their major and trace element compositions are virtually indistinguishable from those of Cr-poor pyropes and off-craton fertile lherzolites, which represent refractory residues after low degrees of partial melting, without subsequent metasomatic overprinting (Suppl. Fig. 6; Ionov et al., 2005b; for major elements see also Griffin et al., 1999a,b,c).

Whatever the origin of Três Ranchos TR10 grt1, TR10 grt2, TR4 grt, TR2b grt, TR2a grt, and TR2c grt1 garnets and Osvaldo Franca

lherzolite-1 garnets, they indicate that the shallowest garnet-facies sector at the southeastern end of the APIP area is rich in fertile lherzolites (possibly associated with pyroxenites, according to the major element composition: see garnet classification). Both at Três Ranchos and at Osvaldo Franca, this fertile lherzolite layer is located at a depth of ~ 100 km. A large fertile layer has been recognized at comparable moderate depths in other cratonic mantle columns (e.g., Griffin et al., 1999b,c, 2002).

The significant contrast between the rather uniform geochemical features arguing for the shallow fertile layer and the heterogeneous chemical features and evolution stages recorded by the underlying peridotites documented by the other Três Ranchos garnets, as well as the variety of deeper garnet groups defined by Carvalho et al., (2022a), suggest that the shallow fertile layer is a very ancient, possibly primary, feature of the Brazilian SCLM.

It is tentatively suggested here that this shallow fertile layer may be the result of regional stacking of mantle slabs with variable compositions during craton formation (see possible analogues mechanisms for the Slave Craton in Griffin et al., 1999b, or of the re-fertilization of the upper part of the Archean lithospheric mantle by interaction with the overlying continental crust (e.g., by crustal delamination), possibly followed by low degrees of partial melting.

Recently, Mulder et al. (2021) suggested that the first Earth cratons were stabilized in Eoarchaean times by mafic underplating with accumulation of juvenile melt at the lower crust - upper mantle interface (see Fig. 4 in Mulder et al., 2021) above persistent rafts of buoyant, melt-depleted mantle. It is proposed here that such a process may have played a role in producing the observed re-fertilization of the shallow Brazilian SCLM, which may thus be a record of the early stages of São Francisco Craton stabilization.

6. Conclusion remarks

The inspection of the petrographic and chemical (major and trace elements) features of garnet and clinopyroxene xenocrysts, and peridotite xenoliths entrained in the Três Ranchos kimberlite has provided valuable insights into the SCLM underneath the APIP, in relation to: (i) the thermal structure and heat flow; (ii) the pristine composition and metasomatic events undergone by the lower SCLM sector; (iii) the nature of the shallow fertile, lherzolite layer. These observations, combined with a reappraisal of the petrochemical data of the Brazilian SCLM, allow to shed light on the stabilization and evolution processes of the São Francisco Craton.

The present-day thickness of the Brazilian SCLM is similar among the Três Ranchos, Canastra, and Osvaldo Franca areas (~ 170 – 180 km depth), although the deep architecture of the SCLM is different according to seismic tomography surveys. In particular, low-velocity anomaly occurs beneath Três Ranchos, whereas the Canastra, and Osvaldo Franca SCLM is characterized by high-velocity anomaly (Rocha et al., 2019). The results of this study suggest that such a scenario was established since the Cretaceous, when the SCLM beneath Três Ranchos became slightly hotter (40 mW/m²), presumably as a consequence of its involvement in the geodynamic evolution of the Brasília Mobile Belt, implying asthenospheric ascent during the nearby Mesozoic to Cenozoic alkaline and tholeiitic magmatism related to the western Gondwana breakup (Ferreira et al., 2022). Differently, the Osvaldo Franca and Canastra SCLM (~ 35 – 36 mW/m²) remained cooler, preserving the stable structure typical of cratonic areas.

The combination of our data with those of the Osvaldo Franca SCLM highlights the occurrence in the São Francisco Craton of i) a deeper sector (>100 km deep beneath Três Ranchos) originally formed by extremely depleted peridotites, which were largely metasomatized by pervasive melt migration of ultra-alkaline silicate melts and/or LILE-enriched fluids; ii) a shallower sector com-

posed by fertile lherzolite apparently unrelated to the evolution processes of the deeper sector.

The effects of percolation of ultra-alkaline silicate melts are particularly widespread in the lowermost sector of the Três Ranchos SCLM.

At a depth of 160 km, two metasomatic events are recorded by chemical and petrographic features in the lherzolite xenolith TR LH1. The first event resulted in the segregation and/or recrystallization of clinopyroxene, documented by a complete geochemical reset of the original, depleted mantle system, during a pervasive, porous-flow melt percolation that developed at very large time-integrated melt-rock ratios. A second melt percolation event caused interstitial segregation of a fine-grained assemblage of phlogopite, perovskite, clinopyroxene, rutile, and ilmenite, and the partial recrystallization/replacement of olivine and pyroxene. The absence of newly formed orthopyroxene, together with clinopyroxene suggests that this second injected melt was silica undersaturated. This event was apparently short-lived, and likely related to the magmatic cycle involving the eruption of the host kimberlite.

The pervasive metasomatism operated by ultra-alkaline melts is recorded up to shallower depths, between 124 and 100 km, where pristine strongly refractory peridotites produced by extreme partial melting (recorded for instance by the HREE composition of TR2c grt2), locally underwent a complete geochemical reset. This is supported by the trace element compositions of the garnet, which approached the equilibrium with the ultra-alkaline metasomatic agent (e.g., TR8 grt1). Modal metasomatism is also documented by phlogopite segregation and /or overgrowth in/on garnets (i.e., TR9 grt and TR2c grt2). Similar information has been reported in the mantle column beneath the Osvaldo Franca 1 kimberlite, where garnets with sinusoidal to spoon shaped REE patterns are attributed to metasomatized depleted peridotites from comparable depths.

Atop the sector composed by metasomatized (\pm phlogopite) and depleted peridotites, at ≤ 100 km depth, the presence of fertile lherzolite is documented by garnet xenocrysts showing lherzolitic major element compositions and linearly fractionated, LREE-depleted, and HREE-enriched pattern. These compositions are typical of kimberlite-borne Cr-poor garnet megacrysts worldwide. This zone is also identified, starting from slightly deeper sectors, beneath the Osvaldo Franca SCLM. Putative metasomatic agents were characterized by significantly lower LREE/HREE ratios than the APIP ultra-alkaline silicate melts (kimberlites and kamafugites). However, the major and trace element compositions of the garnets are virtually indistinguishable from those of Cr-poor garnet megacrysts and of garnets in off-craton fertile lherzolites, which represent refractory residues after low degrees of partial melting, without subsequent metasomatic overprinting. It is expected that interaction between ultra-alkaline melts and shallow fertile lherzolite can develop transitional feature as documented by the LREE-depleted sinusoidal composition of TR8 grt3, which is intermediate between TR8 grt1 and the LREE-depleted garnets. However, the fertile composition of the shallow peridotite likely represented a petrochemical barrier hindering the pervasive percolation of ultra-alkaline melts (Toramaru and Fujii, 1986), in absence of strong thermal erosion imparted by asthenosphere ascent.

In conclusion, the stabilization and evolution of the Brazilian subcontinental lithospheric mantle involved the same chemical and thermal processes observed in other cratonic areas, such as the Kalahari Craton (Griffin et al., 2003). The presence at three localities of the São Francisco Craton (Três Ranchos, Osvaldo Franca, and Brauna) of a relatively shallow mantle portion that does not show obvious relationships with the heterogeneous chemical characteristics and evolutionary stages recorded by the underlying peridotites also seems to be a common feature in many

cratonic lithospheric sections. This suggests that the shallow fertile layer may be a very ancient, possibly primary, feature produced during the early stages of stabilization of the São Francisco Craton.

Declaration of competing interest

The authors declare that they have no known competing financial interests or personal relationships that could have appeared to influence the work reported in this paper.

Acknowledgements

We dedicate this paper to the late Prof. Piero Brotzu and Prof. Darcy Pedro Svisero. They spent their scientific careers in studying Brazilian alkaline and alkaline-carbonatite rocks and were a great guide to VG and RGA work in Brazil. VG is especially grateful to Prof. Brotzu for sharing his love of research and his rigorous approach to petrogenetic modeling. Thanks to Sergio Bravi for his skill in the preparation of the thin sections and to Roberto de' Genaro for his invaluable help with the EDS work. The authors are grateful to Leone Melluso for the samples and his invaluable comments during the preparation of this manuscript. VG would like to thank Prof. M. Santosh, Editor-in-Chief of Gondwana Research. The authors would like to acknowledge the constructive comments of Michel Grégoire and an anonymous reviewer, the constructive comments and advice of Sebastian Tappe, Associate Editor of Gondwana Research, which were very useful in the preparation of this revised manuscript.

Funding sources

The manuscript has benefited of grants from Departmental Research Funds to Vincenza Guarino, from Ministero dell'Università e della Ricerca for funding through Progetti di Ricerca di Interesse Nazionale (PRIN) 2017 [PRIN_20178LPCPW] to Alberto Zanetti, and from Fundação de Amparo à Pesquisa do Estado de São Paulo – FAPESP [2019/22084-8, 2017/03768-8] and the Brazilian National Research Council – CNPq [310055/2021-0; 404020/2021-6] to Rogério Guitarrari Azzone.

Appendix A. Supplementary material

Supplementary data to this article can be found online at <https://doi.org/10.1016/j.gr.2024.01.005>.

References

- Agashev, A.M., Ionov, D.A., Pokhilenko, N.P., Golovin, A.V., Cherepanova, Y., Sharygin, I.S., 2013. Metasomatism in the lithospheric mantle roots: Constraints from WR and minerals chemical composition of deformed peridotite xenoliths from the Udachnaya kimberlite pipe. *Lithos* 160–161, 201–215. <https://doi.org/10.1016/j.lithos.2012.11.014>.
- Almeida, F.F.M., de Brito Neves, B.B., Carneiro, C.D.R., 2000. The origin and evolution of the South American Platform. *Earth-Sci. Rev.* 50, 77–111. [https://doi.org/10.1016/S0012-8252\(99\)00072-0](https://doi.org/10.1016/S0012-8252(99)00072-0).
- Altoe, I., Goes, S., Assumpção, M., 2022. Thermo-compositional structure of the South American Platform lithosphere: Evidence of stability, modification, and erosion. *Geochim. Geophys. Geosystems* 23. <https://doi.org/10.1029/2022GC010516>.
- Anders, E., Grevesse, N., 1989. Abundances of the elements: Meteoritic and solar. *Geochim. Cosmochim. Acta* 53, 197–214. [https://doi.org/10.1016/0016-7037\(89\)90286-X](https://doi.org/10.1016/0016-7037(89)90286-X).
- Artemieva, I.M., Thybo, H., Cherepanova, Y., 2019. Isopycnicity of cratonic mantle restricted to kimberlite provinces. *Earth Planet. Sci. Lett.* 505, 13–19. <https://doi.org/10.1016/j.epsl.2018.09.034>.
- Assumpção, M., Schimmel, M., Escalante, C., Roberto Barbosa, J., Rocha, M., Barros, L. V., 2004. Intraplate seismicity in SE Brazil: stress concentration in lithospheric thin spots. *Geophys. J. Int.* 159, 390–399. <https://doi.org/10.1111/j.1365-246X.2004.02357.x>.
- Aulbach, S., Sun, J., Tappe, S., Höfer, H.E., Gerdes, A., 2017. Volatile-rich metasomatism in the cratonic mantle beneath SW Greenland: Link to kimberlites and mid-lithospheric discontinuities. *J. Petrol.* 58, 2311–2338. <https://doi.org/10.1093/petrology/egy009>.
- Azzone, R.G., Pearson, D.G., Sarkar, C., Chmyz, L., Shibata, C.S.V., Luo, Y., Ruberti, E., 2022. Tracking crustal assimilation processes in kimberlites from the Alto Paranaíba Igneous Province, Brazil: Petrographic and geochemical controls and the role of perovskites. *Lithos* 432–433. <https://doi.org/10.1016/j.lithos.2022.106888>.
- Barabino, G., Gomes, C.B., Traversa, G., 2007. The Lages diatremes: mineral composition and petrological implications. *An. Acad. Bras. Cienc.* 79, 473–501. <https://doi.org/10.1590/S0001-37652007000300010>.
- Bernstein, S., Kelemen, P.B., Hanghøj, K., 2007. Consistent olivine Mg# in cratonic mantle reflects Archean mantle melting to the exhaustion of orthopyroxene. *Geology* 35, 459–462.
- Brod, J.A., Gibson, S.A., Thompson, R.N., Junqueira-Brod, T.C., Seer, H.J., De Moraes, L. C., Boaventura, G.R., 2000. The kamafugite-carbonatite association in the Alto Paranaíba Igneous Province (APIP) southeastern Brazil. *Rev. Brasil. Geocienc.* 30, 404–408.
- Diamante, P., Geológico, S., do Brasil – CPRM. (Eds.), 2017. Áreas Kimberlíticas e Diamantíferas Do Estado De Minas Gerais e Regiões Adjacentes. Programa Geologia Do Brasil, Série Pedras Preciosas, n. 10.
- Canil, D., 1999. The Ni-in-garnet geothermometer: calibration at natural abundances. *Contrib. Mineral. Petrol.* 136, 240–246.
- Carlson, R.W., Esperança, S., Svisero, D.P., 1996. Chemical and Os isotopic study of Cretaceous potassic rocks from Southern Brazil. *Contrib. Mineral. Petrol.* 125, 393–405. <https://doi.org/10.1007/s004100050230>.
- Carsswell, D.A., 1991. The garnet-orthopyroxene Al barometer: problematic application to natural garnet lherzolite assemblages. *Mineral. Mag.* 55, 19–31.
- Carvalho, L.D.V., Jalowitzki, T., Scholz, R., Gonçalves, G.O., Rocha, M.P., Pereira, R.S., Lana, C., de Castro, M.P., Queiroga, G., Fuck, R.A., 2022a. An exotic Cretaceous kimberlite linked to metasomatized lithospheric mantle beneath the southwestern margin of the São Francisco Craton. *Brazil. Geosci. Front.* 13, 101281.
- Carvalho, L.D.V., Stachel, T., Pearson, D.G., Fuck, R.A., Jalowitzki, T., Timmerman, S., Steele-MacInnis, M., Gonçalves, G.O., Silvestre Pereira, R., Scholz, R., 2022b. Diamond formation beneath the Coromandel area, southwestern São Francisco Craton – The role of re-fertilization and subduction. *Lithos* 430–431. <https://doi.org/10.1016/j.lithos.2022.106856>.
- Clement, C.R., 1982. A comparative geological study of some major kimberlite pipes in northern Cape and Orange Free State. University of Cape Town. Ph.D. thesis.
- Coldebella, B., Azzone, R.G., Chmyz, L., Ruberti, E., Svisero, D.P., 2020. Oxygen fugacity of Alto Paranaíba kimberlites and diamond instability: Três Ranchos IV and Limeira I intrusions. *Braz. J. Geol.* 50 (1).
- Costa, V.S., Figueiredo, B.R., Weska, R.K., 1996. Estudos mineralógicos e químicos do kimberlito Batóvi 6 (MT) em comparação com as intrusões Três Ranchos 4 (GO) e Limeira 1 (MG). Ph.D. Thesis, Geochim. Bras. 11 (1).
- Crank, J., 1979. The mathematics of diffusion. Oxford University Press.
- Czas, J., Pearson, D.G., Stachel, T., Kjarsgaard, B.A., Read, G.H., 2020. A Palaeoproterozoic diamond-bearing lithospheric mantle root beneath the Archean Sask Craton. *Canada. Lithos* 356–357, 105301.
- D'Agrella-Filho, M.S., Trindade, R.I.F., Tohver, E., Janikian, L., Teixeira, W., Hall, C., 2011. Paleomagnetism and $^{40}\text{Ar}/^{39}\text{Ar}$ geochronology of the high-grade metamorphic rocks of the Jequié block, São Francisco Craton: Atlantica. Ur and beyond. *Precambrian Res.* 185, 183–201. <https://doi.org/10.1016/j.precamres.2011.01.008>.
- Danni, J.C.M., Gaspar, J.C., Gonzaga, G.M., 1991. The Fazenda Alaginha Intrusion, Três Ranchos, Goiás. CPRM Special Publication.
- Day, H.W., 2012. A revised diamond-graphite transition curve. *Am. Mineral.* 97, 52–62. <https://doi.org/10.2138/am.2011.3763>.
- Donatti-Filho, J.P., Tappe, S., Oliveira, E.P., Heaman, L.M., 2013. Age and origin of the Neoproterozoic Brauna kimberlites: Melt generation within the metasomatized base of the São Francisco craton. *Brazil. Chem. Geol.* 353, 19–35.
- Dymshits, A., Sharygin, I., Liu, Z., Korolev, N., Malkovets, V., Alifirova, T., Yakovlev, I., Xu, I.-G., 2020. Oxidation State of the Lithospheric Mantle Beneath Komsomolskaya-Magnitnaya Kimberlite Pipe, Upper Muna Field. *Siberian Craton. Minerals* 10 (9), 740. <https://doi.org/10.3390/min10090740>.
- Felgate, M.R., 2014. The petrogenesis of Brazilian kimberlites and kamafugites intruded along the 125° lineament: Improved Geochemical and Geochronological Constraints on Magmatism in Rondonia and The Alto Paranaíba Igneous Province. University of Melbourne. Ph.D. thesis.
- Ferreira, A.C.D., Conceição, R.V., Mizusaki, A.M.P., 2022. Mesozoic to Cenozoic alkaline and tholeiitic magmatism related to West Gondwana break-up and dispersal. *Gondwana Res.* 106, 15–33. <https://doi.org/10.1016/j.gr.2022.01.005>.
- Fitzpayne, A., Giuliani, A., Hergt, J., Phillips, D., Janney, P., 2018. New geochemical constraints on the origins of MARID and PIC rocks: Implications for mantle metasomatism and mantle-derived potassic magmatism. *Lithos* 318, 478–493.
- Fulmer, E.C., Nebel, O., van Westrenen, W., 2010. High-precision high field strength element partitioning between garnet, amphibole and alkaline melt from Kakanui. *New Zealand. Geochim. Cosmochim. Acta* 74, 2741–2759.
- Gervasoni, F., Jalowitzki, T., Rocha, M.P., Weska, R.K., Novais-Rodrigues, E., de Freitas Rodrigues, R.A., Bussweiler, Y., Rocha Barbosa, E.S., Berndt, J., Dantes, E.L., da Silva Souza, V., Klemme, S., 2022. Recycling process and proto-kimberlite melt metasomatism in the lithosphere-asthenosphere boundary beneath the Amazonian Craton recorded by garnet xenocrysts and mantle xenoliths from the Carolina kimberlite. *Geosci. Front.* 13, (5) 101429.

- Gibson, S.A., Thompson, R.N., Leonards, O.H., Dickin, A.P., Mitchell, J.G., 1995. The Late Cretaceous impact of the Trindade mantle plume: evidence from large-volume, mafic, potassic magmatism in SE Brazil. *J. Petrol.* 36, 189–229. <https://doi.org/10.1093/petrology/36.1.189>.
- Glaser, S.M., Foley, S.F., Günther, D., 1999. Trace element compositions of minerals in garnet and spinel peridotite xenoliths from the Vitim volcanic field, Transbaikalia, eastern Siberia. In: van der Hilst, R.D., McDonough, W.F., (Eds.), *Development in Geotectonics* 24, 263–285. [Doi: 10.1016/S0419-0254\(99\)80015-9](https://doi.org/10.1016/S0419-0254(99)80015-9).
- Gomes, C.B., Comin-Chiaromonti, P., 2005. Some notes on the Alto Paranaíba igneous province. In: Comin-Chiaromonti, P., Gomes, C.B. (Eds.), *Mesozoic to Cenozoic Alkaline Magmatism in the Brazilian Platform*. FAPESP, São Paulo, Brazil, pp. 317–340.
- Gonzaga, G.M., Tompkins, L.A., 1991. *Geologia do Diamante. Principais Depósitos Minerais Do Brasil* 4, 53–116.
- Gonzaga, G.M., Teixeira, N.A., Gaspar, J.C., 1994. The origin of diamonds in western Minas Gerais. Brazil. *Miner. Depos.* 29, 414–421. <https://doi.org/10.1007/BF01886959>.
- Grégoire, M., Bell, D.R., le Roex, A.P., 2002. Trace element geochemistry of phlogopite-rich mafic mantle xenoliths: their classification and their relationship to phlogopite-bearing peridotites and kimberlites revisited. *Contrib. Mineral. Petrol.* 142, 603–625.
- Grégoire, M., Bell, D.R., le Roex, A.P., 2003. Garnet lherzolites from the Kaapvaal Craton (South Africa): trace element evidence for a metasomatic history. *J. Petrol.* 44, 629–657. <https://doi.org/10.1093/petrology/44.4.629>.
- Griffin, W.L., Kaminsky, F.V., Ryan, C.G., O'Reilly, S.Y., Win, T.T., Ilupin, I.P., 1996. Thermal state and composition of the lithospheric mantle beneath the Daldyn kimberlite field, Yakutia. *Tectonophysics* 262, 19–33.
- Griffin, W.L., Shee, S.R., Ryan, C.G., Win, T.T., Wyatt, B.A., 1999a. Harzburgite to lherzolite and back again: metasomatic processes in ultramafic xenoliths from the Wesselton kimberlite, Kimberley, South Africa. *Contrib. Mineral. Petrol.* 134 (2–3), 232.
- Griffin, W.L., Ryan, C.G., Kaminsky, F.V., O'Reilly, S.Y., Natapov, L.M., Win, T.T., Kinny, P.D., Ilupin, I.P., 1999b. The Siberian lithosphere traverse: mantle terranes and the assembly of the Siberian Craton. *Tectonophysics* 310 (1–4), 1–35.
- Griffin, W.L., Doyle, B.J., Ryan, C.G., Pearson, N.J., O'Reilly, S.Y., Davies, R., Kivi, K., Van Acherbergh, E., Natapov, L.M., 1999c. Layered mantle lithosphere in the Lac de Gras area, Slave craton: composition, structure and origin. *J. Petrol.* 40 (5), 705–727. <https://doi.org/10.1093/petroj/40.5.705>.
- Griffin, W.L., Fisher, N.L., Friedman, J.H., O'Reilly, S.Y., Ryan, C.G., 2002. Cr-pyroxene garnets in the lithospheric mantle 2. Compositional populations and their distribution in time and space. *Geochim. Geophys. Geosystems* 3 (12), 1–35.
- Griffin, W.L., O'Reilly, S.Y., Natapov, L.M., Ryan, C.G., 2003. The evolution of lithospheric mantle beneath the Kalahari Craton and its margins. *Lithos* 71 (2–4), 215–241.
- Grütter, H.S., Gurney, J.J., Menzies, A.H., Winter, F., 2004. An updated classification scheme for mantle-derived garnet, for use by diamond explorers. *Lithos* 77, 841–857. <https://doi.org/10.1016/j.lithos.2004.04.012>.
- Grütter, H., Latti, D., Menzies, A., 2006. Cr-saturation arrays in concentrate garnet compositions from kimberlite and their use in mantle barometry. *J. Petrol.* 47, 801–820. <https://doi.org/10.1093/petrology/egi096>.
- Guarino, V., Brigatti, M.F., 2018. Crystallization conditions of micas in oxidized igneous systems. *Am. Mineral.* 103, 1999–2010. <https://doi.org/10.2138/am-2018-6567>.
- Guarino, V., Wu, F.-Y., Lustrino, M., Melluso, L., Brotzu, P., Gomes, C.B., Ruberti, E., Tassinari, C.C.G., Svisero, D.P., 2013. U-Pb ages, Sr-Nd-isotope geochemistry and petrogenesis of kimberlites, kamafugites and phlogopite-picrites of the Alto Paranaíba Igneous Province. Brazil. *Chem. Geol.* 353, 65–82.
- Guarino, V., Wu, F.-Y., Melluso, L., Gomes, C.B., Tassinari, C.C.G., Ruberti, E., Brill, M., 2017. U-Pb ages, geochemistry, C-O-Nd-Sr-Hf isotopes and petrogenesis of the Catalão II carbonatitic complex (Alto Paranaíba Igneous Province, Brazil): implications for regional-scale heterogeneities in the Brazilian carbonatite associations. *Int. J. Earth Sci.* 106, 1963–1989. <https://doi.org/10.1007/s00531-016-1402-4>.
- Guarino, V., Lustrino, M., Zanetti, A., Tassinari, C.C.G., Ruberti, E., de' Gennaro, R., Melluso, L., 2021. Mineralogy and geochemistry of a giant apatitic magma reservoir: The Late Cretaceous Poços de Caldas potassic alkaline complex (SE Brazil). *Lithos* 398, <https://doi.org/10.1016/j.lithos.2021.106330>.
- Harley, S.L., 1984. An experimental study of the partitioning of Fe and Mg between garnet and orthopyroxene. *Contrib. Mineral. Petrol.* 86, 359–373.
- Hasterok, D., Chapman, D.S., 2011. Heat production and geotherms for the continental lithosphere. *Earth Planet. Sci. Lett.* 307, 59–70.
- Hill, P.J.A., Kopylova, M., Russell, J.K., Cookenboo, H., 2015. Mineralogical controls on garnet composition in the cratonic mantle. *Contrib. Mineral. Petrol.* 169, 13.
- Ionov, D.A., Bodinier, J.L., Mukasa, S.B., Zanetti, A., 2002. Mechanisms and sources of mantle metasomatism: major and trace element compositions of peridotite xenoliths from Spitsbergen in the context of numerical modelling. *J. Petrol.* 43, 2219–2259. <https://doi.org/10.1093/petrology/43.12.2219>.
- Ionov, D.A., Ashchepkov, I., Jagoutz, E., 2005a. The provenance of fertile off-craton lithospheric mantle: Sr-Nd isotope and chemical composition of garnet and spinel peridotite xenoliths from Vitim, Siberia. *Chem. Geol.* 217, 41–75.
- Ionov, D.A., Blichert-Toft, J., Weis, D., 2005b. Hf isotope compositions and HREE variations in off-craton garnet and spinel peridotite xenoliths from central Asia. *Geochim. Cosmochim. Acta* 69, 2399–2418. <https://doi.org/10.1016/j.gca.2004.11.008>.
- Ionov, D.A., Liu, Z., Li, J., Golovin, A.V., Korsakov, A.V., Xu, Y., 2020. The age and origin of cratonic lithospheric mantle: Archean dunites vs. Paleoproterozoic harzburgites from the Udachnaya kimberlite, Siberian Craton. *Geochim. Cosmochim. Acta* 281, 67–90. <https://doi.org/10.1016/j.gca.2020.05.009>.
- Johnson, K.T.M., 1998. Experimental determination of partition coefficients for rare earth and high-field-strength elements between clinopyroxene, garnet, and basaltic melt at high pressures. *Contrib. Mineral. Petrol.* 133 (1–2), 60–68.
- le Roex, A.P., Class, C., 2016. Metasomatic enrichment of Proterozoic mantle south of the Kaapvaal Craton, South Africa: origin of sinusoidal REE patterns in clinopyroxene and garnet. *Contrib. Mineral. Petrol.* 171, 14. <https://doi.org/10.1007/s00410-015-1222-8>.
- Lee, C.T.A., Luffi, P., Chin, E.J., 2011. Building and destroying continental mantle. *Annu. Rev. Earth Planet. Sci.* 39, 59–90.
- Lim, E., Giuliani, A., Phillips, D., Goemann, K., 2018. Origin of complex zoning in olivine from diverse, diamondiferous kimberlites and tectonic settings: Ekati (Canada), Alto Paranaíba (Brazil) and Kaalvallei (South Africa). *Mineral. Petrol.* 112, 539–554. <https://doi.org/10.1007/s00710-018-0607-6>.
- Lima, N.M., Azzone, R.G., Chmyz, L., Guarino, V., Ruberti, E., Silva, S., Svisero, D.P., 2020. Petrographic, geochemical, and isotopic evidence of crustal assimilation processes in the Indaiá-II kimberlite, Alto Paranaíba Province, southeast Brazil. *Can. Mineral.* 58 (5), 563–585. <https://doi.org/10.3749/canmin.2000031>.
- Lyubetskaya, T., Korenaga, J., 2007. Chemical composition of Earth's primitive mantle and its variance: 1. Method and Results. *J. Geophys. Res.* 112, B03211.
- Melluso, L., Lustrino, M., Ruberti, E., Brotzu, P., Gomes, C.B., Morbidelli, L., Morra, V., Svisero, D.P., d'Amelio, F., 2008. Major- and trace-element composition of olivine, perovskite, clinopyroxene, Cr-Fe-Ti oxides, phlogopite and host kamafugites and kimberlites, Alto Paranaíba, Brazil. *Can. Mineral.* 46, 19–40.
- Melluso, L., Scarpatti, C., Zanetti, A., Sparice, D., de' Gennaro, R., 2022. The petrogenesis of chemically zoned, phonolitic, Plinian and sub-Plinian eruptions of Somma-Vesuvius, Italy: Role of accessory phase removal, independently filled magma reservoirs with time, and transition from slightly to highly silica undersaturated magmatic series in an ultrapotassic stratovolcano. *Lithos* 430–431, <https://doi.org/10.1016/j.lithos.2022.106854>.
- Mitchell, R.H., 1986. *Kimberlites: mineralogy, geochemistry and petrology*. Plenum, New York.
- Mulder, J.A., Nebel, O., Gardiner, N.J., Cawood, P.A., Wainwright, A.N., Ivanic, T.J., 2021. Crustal rejuvenation stabilised Earth's first cratons. *Nat. Commun.* 12 (1), 3535. <https://doi.org/10.1038/s41467-021-23805-6>.
- Nickel, K.G., Green, D.H., 1985. Empirical geothermobarometry for garnet peridotites and implications for the nature of the lithosphere, kimberlites and diamonds. *Earth Planet. Sci. Lett.* 73, 158–170.
- Nimis, P., Grütter, H., 2010. Internally consistent geothermometers for garnet peridotites and pyroxenites. *Contrib. Mineral. Petrol.* 159, 411–427.
- Nimis, P., Taylor, W.R., 2000. Single-clinopyroxene thermobarometry for garnet peridotites. Part I. Calibration and testing of a Cr-in-Cpx barometer and an enstatite-in-Cpx thermometer. *Contrib. Mineral. Petrol.* 139, 541–554. <https://doi.org/10.1007/s004100000156>.
- Nimis, P., Zanetti, A., Dencker, I., Sobolev, N.V., 2009. Major and trace element composition of chromian diopsides from the Zagadochnaya kimberlite (Yakutia, Russia): Metasomatic processes, thermobarometry and diamond potential. *Lithos* 112, 397–412. <https://doi.org/10.1016/j.lithos.2009.03.038>.
- Nimis, P., Preston, R., Perritt, S.H., Chinn, I.L., 2020. Diamond's depth distribution systematics. *Lithos* 376, 105729.
- Nowell, G.M., Pearson, D.G., Bell, D.R., Carlson, R.W., Smith, C.B., Kempton, P.D., Noble, S.R., 2004. Hf isotope systematics of kimberlites and their megacrysts: new constraints on their source regions. *J. Petrol.* 45, 1583–1612. <https://doi.org/10.1093/petrology/egh024>.
- Nowicki, T.E., Moore, R.O., Gurney, J.J., Baumgartner, M.C., 2007. Diamonds and associated heavy minerals in kimberlite: a review of key concepts and applications. *Dev. Sedimentol.* 58, 1235–1267. [https://doi.org/10.1016/S0070-4571\(07\)58046-5](https://doi.org/10.1016/S0070-4571(07)58046-5).
- Nowicki, T., Porritt, L., Crawford, B., Kjarsgaard, B., 2008. Geochemical trends in kimberlites of the Ekati property, Northwest Territories, Canada: Insights on volcanic and resedimentation processes. *J. Volcanol. Geotherm. Res.* 174, 117–127. <https://doi.org/10.1016/j.jvolgeores.2007.12.030>.
- Patterson, M., Francis, D., McCandless, T., 2009. Kimberlites: magmas or mixtures? *Lithos* 112, 191–200. <https://doi.org/10.1016/j.lithos.2009.06.004>.
- Pearce, N.J., Perkins, W.T., Westgate, J.A., Gorton, M.P., Jackson, S.E., Neal, C.R., Chenev, S.P., 1997. A compilation of new and published major and trace element data for NIST SRM 610 and NIST SRM 612 glass reference materials. *Geostand. Newsl.* 21, 115–144. <https://doi.org/10.1111/j.1751-908X.1997.tb00538.x>.
- Pereira, R.S., 2007. *Cráton do São Francisco, kimberlitos e diamantes*. PhD thesis. Universidade de Brasília, Brasília. 200 pp (in Portuguese).
- Peucat, J.-J., Barbosa, J.S.F., de Araújo Pinho, I.C., Paquette, J.-L., Martin, H., Fanning, C.M., de Menezes Leal, A.B., Cruz, S., 2011. Geochronology of granulites from the south Itabuna-Salvador-Curaçá Block, São Francisco Craton (Brazil): Nd isotopes and U-Pb zircon ages. *J. S. Am. Earth Sci.* 31, 397–413. [Doi: 10.1016/j.jsames.2011.03.009](https://doi.org/10.1016/j.jsames.2011.03.009).
- Piccardo, G.B., Zanetti, A., Müntener, O., 2007. Melt/peridotite interaction in the Southern Lanzo peridotite: Field, textural and geochemical evidence. *Lithos* 94, 181–209.
- Pouchou, J.L., Pichoir, F., 1988. A simplified version of the 'PAP' model for matrix corrections in EPMA. In: Newbury D. (Ed.), *Microbeam Analysis*. San Francisco Press, 315–318.

- Priestley, K., McKenzie, D., Ho, T., 2018. A lithosphere-asthenosphere boundary-A global model derived from multimode surface-wave tomography and petrology. In: Yuan, H., Romanowicz, B., (Eds.), *Lithospheric discontinuities*, 111–125. Doi: 10.1002/9781119249740.ch6.
- Ragozin, A.L., Agashev, A.M., Zedgenizov, D.A., Denisenko, A.A., 2021. Evolution of the Lithospheric Mantle beneath the Nakyn Kimberlite Field: Evidence from Garnets in the Peridotite Xenoliths of the Nyurba and Botuoba Pipes. *Geochem. Int.* 59 (8), 743–756. <https://doi.org/10.1134/S0016702921080061>.
- Read, G., Grutter, H., Winter, S., Luckman, N., Gaunt, F., Thomsen, F., 2004. Stratigraphic relations, kimberlite emplacement and lithospheric thermal evolution, Quiricó Basin, Minas Gerais State, Brazil. *Lithos* 77, 803–818. <https://doi.org/10.1016/j.lithos.2004.04.011>.
- Reisberg, L., Lorand, J.P., 1995. Longevity of sub-continental mantle lithosphere from osmium isotope systematics in orogenic peridotite massifs. *Nature* 376 (6536), 159–162.
- Rocha, M.P., Assumpção, M., Affonso, G.M.P.C., Azevedo, P.A., Bianchi, M., 2019. Teleseismic P-wave Tomography Beneath the Pantanal, Paraná, and Chaco-Paraná Basins, SE South America: Delimiting Lithospheric Blocks of the SW Gondwana Assemblage. *J. Geophys. Res. Solid Earth* 124, 7120–7137. <https://doi.org/10.1029/2018JB016807>.
- Rodrigues, de F.R.A., Gervasoni, F., Jalowitzki, T., Bussweiler, Y., Berndt, J., Botelho, N. F., Queiroga, G., de Castro, M.P., da Silva, S.W., Ciriaco B.A., de Oliveira, I.L., Klemme, S., 2023. Mantle metasomatism and refertilization beneath the SW margin of the São Francisco Craton, Brazil. *Lithos* 448, 107164.
- Ryan, C.G., Griffin, W.L., Pearson, N.J., 1996. Garnet geotherms: Pressure-temperature data from Cr-pyrope garnet xenocrysts in volcanic rocks. *J. Geophys. Res.* 101, 5611–5625.
- Schulze, D.J., 2003. A classification scheme for mantle-derived garnets in kimberlite: a tool for investigating the mantle and exploring for diamonds. *Lithos* 71, 195–213. [https://doi.org/10.1016/S0024-4937\(03\)00113-0](https://doi.org/10.1016/S0024-4937(03)00113-0).
- Shaikh, A.M., Tappe, S., Bussweiler, Y., Patel, S.C., Ravi, S., Bolhar, R., Viljoen, F., 2020. Clinopyroxene and garnet mantle cargo in kimberlites as probes of Dharwar Craton architecture and geotherms, with implications for post-1.1 Ga lithosphere thinning events beneath Southern India. *J. Petrol.* 61 (9), egaa087. <https://doi.org/10.1093/petrology/egaa087>.
- Shchukina, E.V., Agashev, A.M., Pokhilenko, N.P., 2017. Metasomatic origin of garnet xenocrysts from the V. Grib kimberlite pipe, Arkhangelsk region, NW Russia. *Geosci. Front.* 8 (4), 641–651. <https://doi.org/10.1016/j.gsf.2016.08.005>.
- Shchukina, E.V., Agashev, A.M., Shchukin, V.S., 2019. Diamond-bearing root beneath the northern East European platform (Arkhangelsk region, Russia): Evidence from Cr-pyrope trace-element geochemistry. *Minerals* 9 (5), 261. <https://doi.org/10.3390/min9050261>.
- Shirey, S.B., Walker, R.J., 1998. The Re-Os isotope system in cosmochemistry and high-temperature geochemistry. *Ann. Rev. Earth Planet. Sci.* 26, 423–500.
- Shu, Q., Brey, G.P., 2015. Ancient mantle metasomatism recorded in subcalic garnet xenocrysts: Temporal links between mantle metasomatism, diamond growth and crustal tectonomagmatism. *Earth Planet. Sci. Lett.* 418, 27–39. <https://doi.org/10.1016/j.epsl.2015.02.038>.
- Sparks, R.S.J., Baker, L., Brown, R.J., Field, M., Schumacher, J., Stripp, G., Walters, A., 2006. Dynamical constraints on kimberlite volcanism. *J. Volcanol. Geotherm. Res.* 155, 18–48. <https://doi.org/10.1016/j.jvolgeores.2006.02.010>.
- Stachel, T., Harris, J.W., 2008. The origin of cratonic diamonds - Constraints from mineral inclusions. *Ore Geol. Rev.* 34 (1–2), 5–32. <https://doi.org/10.1016/j.oregeorev.2007.05.002>.
- Stachel, T., Viljoen, K.S., Brey, G., Harris, J.W., 1998. Metasomatic processes in lherzolitic and harzburgitic domains of diamondiferous lithospheric mantle. *Earth Planet. Sci. Lett.* 159, 1–12. [https://doi.org/10.1016/S0012-821X\(98\)00064-8](https://doi.org/10.1016/S0012-821X(98)00064-8).
- Sudholz, Z.J., Yaxley, G.M., Jaques, A.L., Chen, J., 2021. Ni-in-garnet geothermometry in mantle rocks: a high pressure experimental recalibration between 1100 and 1325° C. *Contrib. Mineral. Petrol.* 176, 1–16.
- Sudholz, Z.J., Green, D.H., Yaxley, G.M., Jaques, A.L., 2022. Mantle geothermometry: Experimental evaluation and recalibration of Fe-Mg geothermometers for garnet-clinopyroxene and garnet-orthopyroxene in peridotite, pyroxenite and eclogite systems. *Contrib. Mineral. Petrol.* 177 (8), 77.
- Sun, C., Dasgupta, R., 2020. Thermobarometry of CO₂-rich, silica-undersaturated melts constrains cratonic lithosphere thinning through time in areas of kimberlitic magmatism. *Earth Planet. Sci. Lett.* 550, <https://doi.org/10.1016/j.epsl.2020.116549>.
- Takenaka, L.B., Förster, M.W., Alard, O., Griffin, W.L., Jacob, D.E., Basei, M.A., O'Reilly, S.Y., 2023. Multi-mineral geochronology of kimberlites, kamafugites and alkaline-carbonatite rocks, SW São Francisco Craton, Brazil: Appraisal of intrusion ages. *Gondwana Res.* 124, 246–272.
- Tappe, S., Smart, K., Torsvik, T., Massuyeau, M., de Wit, M., 2018. Geodynamics of kimberlites on a cooling Earth: Clues to plate tectonic evolution and deep volatile cycles. *Earth Planet. Sci. Lett.* 484, 1–14.
- Tappe, S., Budde, G., Stracke, A., Wilson, A., Kleine, T., 2020. The tungsten-182 record of kimberlites above the African superplume: Exploring links to the core-mantle boundary. *Earth Planet. Sci. Lett.* 547, 116473.
- Tappe, S., Massuyeau, M., Smart, K.A., Woodland, A.B., Gussone, N., Milne, S., Stracke, A., 2021. Sheared peridotite and megacryst formation beneath the Kaapvaal craton: A snapshot of tectonomagmatic processes across the lithosphere-asthenosphere transition. *J. Petrol.* 62, 1–39.
- Tilhac, R., Begg, G.C., O'Reilly, S.Y., Griffin, W.L., 2022. A global review of Hf-Nd isotopes: New perspectives on the chicken-and-egg problem of ancient mantle signatures. *Chem. Geol.* 121039. <https://doi.org/10.1016/j.chemgeo.2022.121039>.
- Toramaru, A., Fujii, N., 1986. Connectivity of melt phase in a partially molten peridotite. *J. Geophys. Res. Solid Earth* 91 (B9), 9239–9252.
- Van Acherterbergh, E., Ryan, C.G., Griffin, W.L., 2001. GLITTER on-line interactive data reduction for the LA-ICPMS microprobe. Macquarie Research Ltd., Sydney.
- Warr, L.N., 2021. IMA-CNMNC approved mineral symbols. *Mineral. Mag.* 85 (3), 291–320. <https://doi.org/10.1180/mgm.2021.43>.
- Zack, T., Foley, S.F., Jenner, G.A., 1997. A consistent partition coefficient set for clinopyroxene, amphibole and garnet from laser ablation microprobe analysis of garnet pyroxenites from Kakanui, New Zealand. *Neues Jahrb. Fur Mineral. Abh.* 172 (1), 23–41.
- Ziberna, L., Klemme, S., Nimis, P., 2013a. Garnet and spinel in fertile and depleted mantle: insights from thermodynamic modelling. *Contrib. Mineral. Petrol.* 166, 411–421. <https://doi.org/10.1007/s00410-013-0882-5>.
- Ziberna, L., Nimis, P., Zanetti, A., Marzoli, A., Sobolev, N.V., 2013b. Metasomatic processes in the central Siberian cratonic mantle: evidence from garnet xenocrysts from the Zagadochnaya kimberlite. *J. Petrol.* 54, 2379–2409.
- Ziberna, L., Nimis, P., Kuzmin, D., Malkovets, V.G., 2016. Error sources in single-clinopyroxene thermobarometry and a mantle geotherm for the Novinka kimberlite, Yakutia. *Am. Mineral.* 101, 2222–2232. <https://doi.org/10.2138/am-2016-5540>.